HAW HAMBURG

Master Thesis

Dennis Camilo

Comparing Aircraft Wake Turbulence Categories with Induced Power Calculation

Fakultät Technik und Informatik

Department Fahrzeugtechnik und Flugzeugbau

Faculty of Engineering and Computer Science

Department of Automotive and Aeronautical Engineering

Dennis Camilo

Comparing Aircraft Wake Turbulence Categories with Induced Power Calculation

Master Thesis submitted as part of the master examination

in the degree course Aeronautical Engineering
at the Department of Automotive and Aeronautical Engineering
of the Faculty of Engineering and Computer Science
at Hamburg University of Applied Sciences

First examiner: Prof. Dr.-Ing. Dieter Scholz
Second examiner: Prof. Dr.-Ing. Martin Wagner

Submitted: 30.12.2022

DOI:
https://doi.org/10.15488/xxxxx

URN:
https://nbn-resolving.org/urn:nbn:de:gbv:18302-aero2022-12-30.011
Associated URLs:
https://nbn-resolving.org/html/urn:nbn:de:gbv:18302-aero2022-12-30.011

Any further request may be directed to:
Prof. Dr.-Ing. Dieter Scholz, MSME
E-Mail see: http://www.ProfScholz.de

This work is part of:
Digital Library - Projects & Theses - Prof. Dr. Scholz
http://library.ProfScholz.de

Published by
Aircraft Design and Systems Group (AERO)
Department of Automotive and Aeronautical Engineering
Hamburg University of Applied Science

This report is deposited and archived:
- Deutsche Nationalbiliothek (https://www.dnb.de)
- Repositorium der Leibniz Universität Hannover (https://www.repo.uni-hannover.de)
- Internet Archive (https://archive.org)
  Item: https://archive.org/details/TextCamilo.pdf

This report has associated published data in Harvard Dataverse:
https://doi.org/10.7910/DVN/JC31A0

Name of student
Dennis Camilo

Title of the report
Comparing Aircraft Wake Turbulence Categories with Induced Power Calculation

Keywords (LCSH)
Aeronautics, Airplanes, Aerospace engineering, Airplanes--Performance, Aerodynamics, Drag (Aerodynamics), Airplane--Wings, Vortex shedding

Abstract

Purpose – Definition of new Wake Turbulence Categories (WTC) based on the calculation of induced power of aircraft on approach. This requires the parameters aircraft mass, span, approach speed, air density, and Oswald factor (calculated from wing aspect ratio, wing sweep, wing taper ratio, winglet height, and fuselage diameter). This is considerably more detailed than other metrics based on aircraft mass only or aircraft mass together with wing span.
Methodology – 89 different aircraft are selected which vary significantly in their parameters. Parameters are determined from the Internet; Oswald factor and induced power is calculated. Suitable boundaries of the new WTC (CAT I, II, III, IV) are determined based on induced power. Aircraft with their new categories are presented and compared to FAA, EUROCONTROL, CAA and ICAO WTCs.
Findings – Induced power can be derived not only from induced drag (as a function of lift), but also from the energy in the vortex. When compared to FAA, EUROCONTROL, CAA and ICAO WTC, the new Wake Turbulence Categories seems to offer categorization with more consistency.
Research Limitations – New (reduced) wake separation minima are not considered. Physics based separation minima would need a double classification of each aircraft: a) classification related to wake vortex generation as done here and b) classification related to rolling resistance. Wake separation minima would then be allocated from a pairwise comparison.
Practical Implications – Physics based WTC may categorize more reliable, which increases safety when applied to given separation minima.
Originality – Induced power has not been used as metric for wake turbulence before.

Name des Studierenden
Dennis Camilo

Thema der Masterarbeit
Vergleich von Wirbelschleppen-Kategorien von Flugzeugen mit der Berechnung der induzierten Leistung

Stichworte (GND)
Luftfahrt, Luftfahrzeug, Flugmechanik, Aerodynamik, Passagierflugzeug, Wirbelschleppe, Leistung, Flügel, Spannweite

Kurzreferat

Zweck – Definition neuer Wake Turbulence Categories (WTC) basierend auf der Berechnung der induzierten Leistung von Flugzeugen beim Anflug. Dazu werden die Parameter Flugzeugmasse, Spannweite, Anfluggeschwindigkeit, Luftdichte und Oswald-Faktor (berechnet aus Flügelstreckung, Flügelpfeilung, Flügelzuspitzung, Winglethöhe und Rumpfdurchmesser) benötigt. Dies ist erheblich detaillierter als andere Metriken, die nur auf der Flugzeugmasse oder der Flugzeugmasse zusammen mit der Spannweite basieren.
Methodik – Es werden 89 verschiedene Flugzeuge ausgewählt, die sich in ihren Parametern stark unterscheiden. Parameter werden aus dem Internet ermittelt, Oswaldfaktor und induzierte Leistung werden berechnet. Geeignete Grenzen der neuen WTC (CAT I, II, III, IV) werden basierend auf der induzierten Leistung bestimmt. Flugzeuge mit ihren neuen Kategorien werden vorgestellt und mit WTCs von FAA, EUROCONTROL, CAA und ICAO verglichen.
Ergebnisse – Die induzierte Leistung kann nicht nur aus dem induzierten Widerstand (als Funktion des Auftriebs), sondern auch aus der Energie im Wirbel abgeleitet werden. Im Vergleich zu FAA, EUROCONTROL, CAA und ICAO WTC scheinen die neuen Wake Turbulence-Kategorien eine konsistentere Kategorisierung zu bieten.
Grenzen der Anwendbarkeit – Eine neue Staffelung mit reduzierten Abständen wird nicht betrachtet. Eine physikalisch basierte Staffelung würden eine doppelte Klassifikation jedes Flugzeugs erfordern: a) eine Klassifikation bezogen auf Wirbelschleppenerzeugung wie hier durchgeführt und b) eine Klassifikation bezogen auf dem Beharrungsvermögen hinsichtlich des Rollens um die X-Achse. Eine Staffelung würde sich dann aus einem paarweisen Vergleich ergeben.
Bedeutung für die Praxis – WTCs auf Basis der Physik können eine zuverlässigere Einteilung bringen. Das erhöht die Sicherheit, wenn die Einteilung auf gegebenen Mindestabständen beruht.
Originalität – Induzierte Leistung wurde bisher nicht als Maß für Wirbelschleppen verwendet.

DEPARTMENT OF AUTOMOTIVE AND AERONAUTICAL ENGINEERING

Comparing Aircraft Wake Turbulence Categories with Induced Power Calculation

Task for a *Master Thesis*

Background

Aircraft produce wake turbulence or wake vortex turbulence. The whole topic is covered here with many articles. Depending on their vortex strength, aircraft are put in categories. The criteria for the categories vary. ICAO goes by aircraft mass and lists aircraft by category. EUROCONTROL goes by aircraft mass and wing span (Figure 6) and also lists aircraft by category (Table 2). Also, the FAA lists aircraft by category (Table A-1). Flight mechanics on the topic can be quite simple. The vortex strength can be calculated with what we call "induced power". I have explained it here.

Task

Your task is

- to perform a small systematic literature review on the term "induced power" (you may not find much),
- to select a number of aircraft that are sufficiently different in maximum take-off mass, wing span and other characteristics (include in your list also aircraft that are known to have special characteristics like B757 and A380, include in your list aircraft that are in the list of ICAO, FAA, and EUROCONTROL),
- to determine the relevant parameters for your aircraft (as they are necessary to calculate "induced power"), e.g. maximum landing mass, wing span, approach speed, and estimate the Oswald factor,
- to calculate "induced Power" of the selected aircraft on approach,
- to compare the calculated "induced Power" with the official categories from ICAO, FAA, and EUROCONTROL,
- to draw your conclusions,
- to define your own Wake Turbulence Categories (WTC).

The report has to be written in English based on German or international standards on report writing.

Table of Contents

List of Figures

List of Tables

List of Symbols

A	aspect ratio
b	wing span
$C_{D,0}$	zero drag coefficient
C_{fe}	skin friction coefficient
C_L	lift coefficient
D_i	induced drag
d_F	fuselage diameter
E_k	kinetic energy per unit length
e_{theo}	theoretical Oswald factor
e	Oswald factor
g	gravitational acceleration
h	winglet height
I_x	moment of inertia about the x-axis
k_{e,D_0}	correction factor (viscous drag)
$k_{e,F}$	correction factor (fuselage)
$k_{e,M}$	correction factor (compressibility)
$k_{e,WL}$	correction factor (winglets)
L_R	rolling moment
L	lift force
m	aircraft mass
P_{wake}	induced power
$\dot{p}$	roll acceleration
r_c	vortex core radius
S_W	reference wing area
S_{wet}	wetted aircraft area
S	wing area
V	airspeed

Greek Symbols

φ_{25}	quarter chord sweep
Γ	circulation
λ	taper ratio
ρ	air density

List of Abbreviations

AVOSS	Aircraft Vortex Spacing System
CAA	Civil Aviation Authority
FAA	Federal Aviation Administration
HAW	Hochschule für Angewandte Wissenschaften Hamburg (Hamburg University of Applied Sciences)
ICAO	International Civil Aviation Organization
MTOW	Maximum Takeoff Weight
MW	Megawatt
NASA	National Aeronautics and Space Administration
PCDL	Pulsed Coherent Doppler Lidar
WSVBS	Wirbelschleppen-Vorhersage- und -Beobachtungssystem (Wake Vortex Prediction and Monitoring System)
WTC	Wake Turbulence Category

1 Introduction

1.1 Motivation

One of the biggest challenges for aviation in the upcoming years will certainly be the increasing number of passengers and, consequently, the increasing number of aircraft movements. Airspace and, above all, airport capacities are limited.

At the same time, aircraft must maintain a certain separation to avoid encountering wake vortices from aircraft flying ahead, which in the worst case can endanger flight safety. Wake vortices are an unavoidable consequence of an aircraft generating lift and must thus always be considered.

The challenge therefore is to categorize aircraft into wake turbulence categories as precisely as feasible to enable as many aircraft movements as possible, but at the same time to ensure that flight safety is always the utmost priority.

The criteria for categorizing aircraft wake turbulence differ. Most commonly, aircraft mass and wingspan are considered to classify aircraft into wake turbulence categories. In this thesis the objective is to use other variables related to flight mechanics and aircraft design to calculate induced power and to categorize aircraft into new wake turbulence categories based on these calculations.

With improved categorization, minimum separation distances can be optimized in the ideal case, allowing the number of flight movements to be increased. However, this thesis only aims to improve wake turbulence categorization and does not address the reduction of wake separation minima.

1.2 Title Terminology

The title of this thesis is “Comparing Aircraft Wake Turbulence Categories with Induced Power Calculation”. Following is a definition of each of the terms found in the title.

Comparison
Longman 2022a defines the term comparison as follows:

> *The process of comparing two or more people or things.*

Aircraft
The term aircraft is defined in Longman 2022b as follows:

A plane or other vehicle that can fly.

Wake Turbulence
SKYbrary 2022b defines wake turbulence as follows:

Wake ... Turbulence is defined as turbulence which is generated by the passage of an aircraft in flight.

Categories
In Merriam-Webster 2022 the term categories is defined as follows:

Any of several fundamental and distinct classes to which entities or concepts belong.

Induced Power
In Scholz 2022 the term induced power is defined as follows:

The power an aircraft continually contributes to its wake vortex.

Calculation
Longman 2022c defines the term calculation as follows:

When you use numbers in order to find out an amount, price, or value.

1.3 Objectives

The objective of this thesis is to define new Wake Turbulence Categories based on induced power calculation and compare them to the categories which are used by EUROCONTROL, FAA, CAA, and the ICAO to classify wake turbulence.

For this purpose, the induced power of several aircraft that vary significantly in mass, wingspan and other characteristics will be calculated. Based on the results of these calculations new Wake Turbulence Categories will be defined and compared to conventional Wake Turbulence Categories.

1.4 Literature Review

One important reference source is the master's thesis from Liu 2007**.** Information about wake encounter scenarios, parameters affecting the wake encounter and vortex models have been obtained from this thesis.

The paper Breitsamter 2010 was used to obtain information about the generation of wake vortices, encounter scenarios and the stages of wake vortex lifespan.

The equation for the calculation of induced power is derived from Scholz 2022. The equations and methods for the estimation of the Oswald factor are obtained from Nita 2012.

Various sources were used for the required input parameters for the calculations in this thesis, which are indicated in the Excel file containing the calculations.

1.5 Structure

This thesis consists of seven chapters with the following structure:

Chapter 2 A review of the research on wake vortices is presented in this chapter.

Chapter 3 This chapter explains the theoretical basics of wake turbulence. It is addressed how wake turbulence is generated, and which factors influence a wake encounter. Also, an insight is given into wake turbulence classification systems and vortex models.

Chapter 4 In this chapter the methodology for the calculation of induced power is explained.

Chapter 5 The results of the induced power calculation are presented in this chapter. The new wake turbulence categories defined based on this calculation are then being compared to conventional wake turbulence classification systems.

Chapter 6 The main results of this thesis are summarized and concluded.

Chapter 7 This chapter presents recommendations for further research and another possible categorization for wake turbulence based on the induced power calculation.

Additional research data for this thesis is separately available at Harvard Dataverse which can be accessed here: https://doi.org/10.7910/DVN/JC31A0.

2 Literature Review

For the literature research within this thesis, the search term “induced power” was initially used. The only noteworthy literature found through this search is Anderson 1999 which explains the fundamentals of induced power. Apart from this paper the search did not provide any significant literature related to wake turbulence; therefore, the search was expanded to include the search term “wake vortex”. The search for wake vortex leads to extensive literature resources on wake vortex research, which are presented below.

A significant research subject within wake vortex research covers the generation and dissipation mechanisms of wake vortices. In Rossow 1999 a comprehensive overview of research on wake vortex generation and dissipation mechanisms by conducting numerous experiments and observations is presented.

In Holzäpfel 2003b a probabilistic two-phase wake vortex decay model (P2P) is proposed which predicts the behavior of wake vortices depending on environmental and aircraft parameters. In another paper Holzäpfel 2003c studies wake vortex evolution and decay mechanisms in various atmospheric conditions. This includes the research on the turbulent decay of wake vortices in thermally stably stratified environments in Holzäpfel 2001.

Another research subject addresses the topic of wake encounters and the safety assessment of wake encounters for following aircraft which is covered in Rossow 1999 as well. In Bienik 2007 different wake encounter scenarios, which are defined by using various parameters, are analyzed. Speijker 2007 also analyzes wake encounters and in addition provides a safety assessment for aircraft encountering wake turbulence. In Liu 2007 wake encounters are also being analyzed using a self-programmed code based on the Vortex Lattice Method (VLM) to calculate the rolling moment induced on an aircraft flying through the wake of another aircraft.

Furthermore, another subject within wake vortex research addresses the prediction and monitoring of wake vortices. In Holzäpfel 2009 the wake vortex prediction and monitoring system WSVBS is presented which aims to increase airport capacity with closely spaced parallel runways by adjusting aircraft separations depending on environmental conditions. In Gerz 2009 this wake vortex prediction system is applied in practice on the example of Frankfurt Airport. Another wake vortex prediction system called Aircraft Vortex Spacing System (AVOSS) was developed by NASA and is described in Robins 2002. Like WSVBS, AVOSS aims to determine safe aircraft separations based on actual environmental and vortex-detection data.

In order to establish a wake vortex prediction and monitoring system it is necessary to obtain valid wake-detection data. In Holzäpfel 2003a methods to detect wake vortices are presented using Lidar. In Liu 2021 a pulsed coherent Doppler lidar (PCDL) is used to observe wake vortex evolution under crosswind conditions.

With ever advancing research, continuous efforts are being made to reduce wake separation minima with the objective of enabling as many aircraft movements as possible. Pan 2022 analyses to which extent wake separation can be reduced and how the reduction of separation effects the safety of succeeding aircraft encountering the wake turbulence.

It is also important to mention the specialty regarding the Wake Turbulence Category of the A380 discussed in Scholz 2022. Due to its large weight, the A380 is assigned by ICAO to the specially created WTC Super which is explained in Section 3.5.1. Following aircraft must therefore maintain a greater separation distance compared to aircraft in the WTC Heavy. Before the A380 had its first flight, there were efforts by various stakeholders, like airlines, pilots, or airports, to ensure that the A380 would be assigned to the existing WTC Heavy. An assignment to WTC Super results in a decrease of an airport's approach capacity due to the larger separation. The expected advantage of being able to fill slots with a maximum number of passengers is therefore relativized by this classification. Within this thesis it shall be discussed how the decision of ICAO to define a new WTC for the A380 is to be evaluated.

Another notable specialty is the classification of the B757 into a Wake Turbulence Category. According to the ICAO categorization, the WTC Medium is assigned. However, explained in SKYbrary 2022a, some states use the WTC Heavy for the B757 being the only narrowbody aircraft with this classification. The FAA also has a separate WTC category for the B757. Therefore, also evaluated in this thesis is the extent to which the different treatment of the B757 is appropriate.

The literature review proves that in recent years substantial research has been conducted and is still being done on the subject of wake vortices. There is a good understanding of the generation and dissipation mechanisms of wake vortices. It is also possible to provide precise assessments regarding the hazards of wake encounters. Through wake-detection and utilization of real-time weather data wake vortices can be predicted and monitored extensively. Despite this far advanced research, the categorization of aircraft into Wake Turbulence Categories, which is covered in the next chapter, is rather rudimentary. The objective of this thesis will therefore be categorizing aircraft into WTC more precisely, considering other variables than just the aircraft mass or wing span.

3 Theoretical Basics

Wake turbulence is defined in SKYbrary 2022b as disturbance in the atmosphere which is generated by the passage of an aircraft in flight. This turbulence in the wake of an aircraft in flight is principally caused by wing tip vortices. In the following section, the physical fundamentals of wake vortices are described further, as well as the categorization of wake turbulence.

3.1 Creation of Wake Turbulence

As described in Breitsamter 2010 wake turbulence is a direct and natural consequence of the generation of lift by a wing. The fundamental principle for generating lift is that the airflow along the bottom of the wing is less accelerated than the flow on the upper side of the wing. According to Bernoulli's principle that the pressure in a fluid is reduced as the speed of the flow is increased this results in the pressure on the bottom side being greater relative to the upper side of the wing.

Since the span of the wing is finite there is a flow around the wing tip as a result of the pressure difference and the subsequent aim to equate this state. This results in a strong vortex, which is referred to as "wing tip vortex". Between both counter-rotating wing tip vortices a vortex sheet with downward velocities or downwash develops.

Depending on the ambient conditions, these vortices last for up to several minutes spreading laterally from the aircraft while they continue to descend and decay gradually due to instability and atmospheric effects. The wake vortex behind a lifting wing is depicted in Figure 3.1 and Figure 3.2.

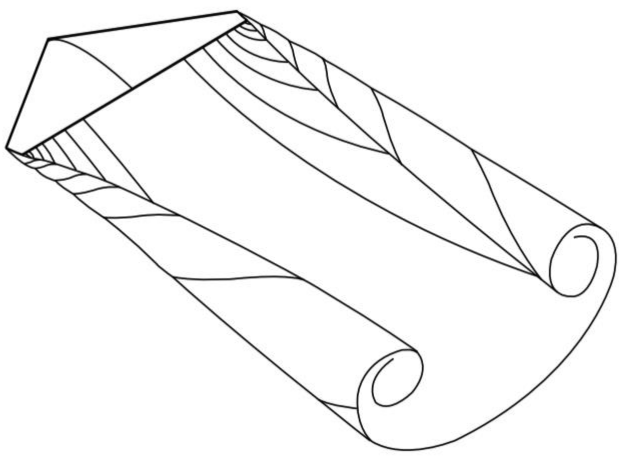

Figure 3.1 The vortex wake behind a lifting wing (McLean 2005)

Figure 3.2 Visible vortices behind a flying aircraft (Rill 1996)

According to Breitsamter 2010 the wake of an aircraft can be divided into four sections. The near field is the area in which highly concentrated vortices form. The second region is the extended near field. Here the wake vortices begin to roll up. Also, different co-vortices merge in this area leading to two counter-rotating vortices at the end of the extended near field. In the mid and far field the vortices begin to descend and gradually decay in the atmosphere. In the decay or dispersion region the two vortices finally fully decay and collapse due to instabilities. The different stages of the vortex wake are shown in Figure 3.3.

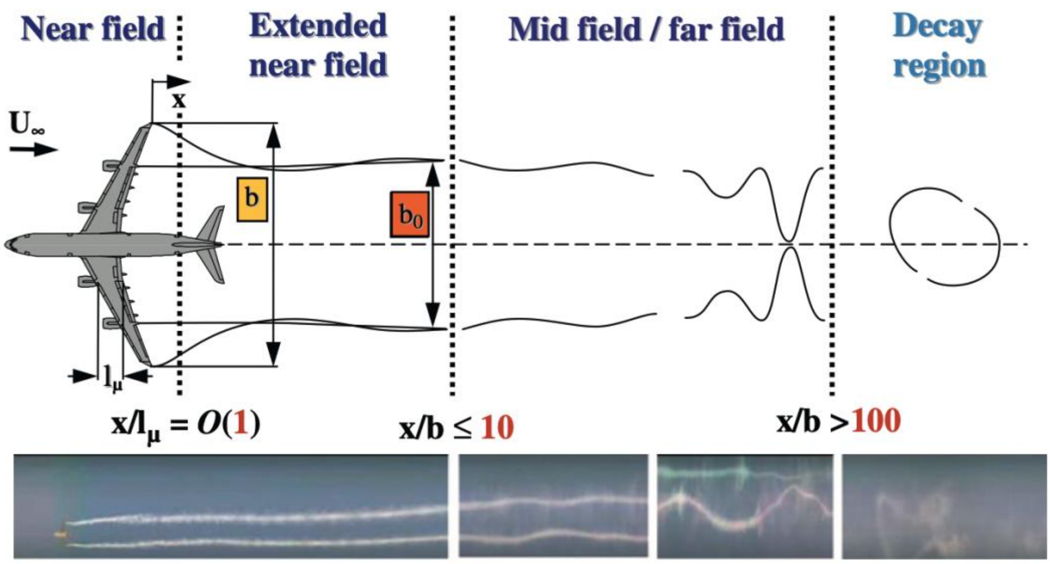

Figure 3.3 Stages of the vortex wake behind an aircraft (Breitsamter 2010)

3.2 Influencing Factors

There are several factors to be considered when assessing the impact of wake vortices on following aircraft. Figure 3.4 shows the different correlations according to Liu 2007. The aircraft design and operational characteristics of the generating or leading aircraft, like weight, span, span load and stall speed, determine the generation of the wake vortices and their roll-up. The flight conditions of the leading aircraft, specifically the velocity and air density, also influence the roll-up of wake vortices.

Weather conditions, like wind direction, wind speed, turbulence, and temperature profile, have an impact on the vortex aging and the duration wake vortices persist. Slow windspeeds and stable weather conditions favor an extended survival duration.

The characteristics of the aged wake vortex and the properties of the following aircraft, including speed, wing span, intercept route, aspect, and taper ratio, eventually determine the impact of wake vortices on the trailing aircraft. In this thesis, in order to recategorize wake turbulence, only the characteristics of the leading aircraft are considered. External factors, like weather conditions or the air traffic management, are not taken into account.

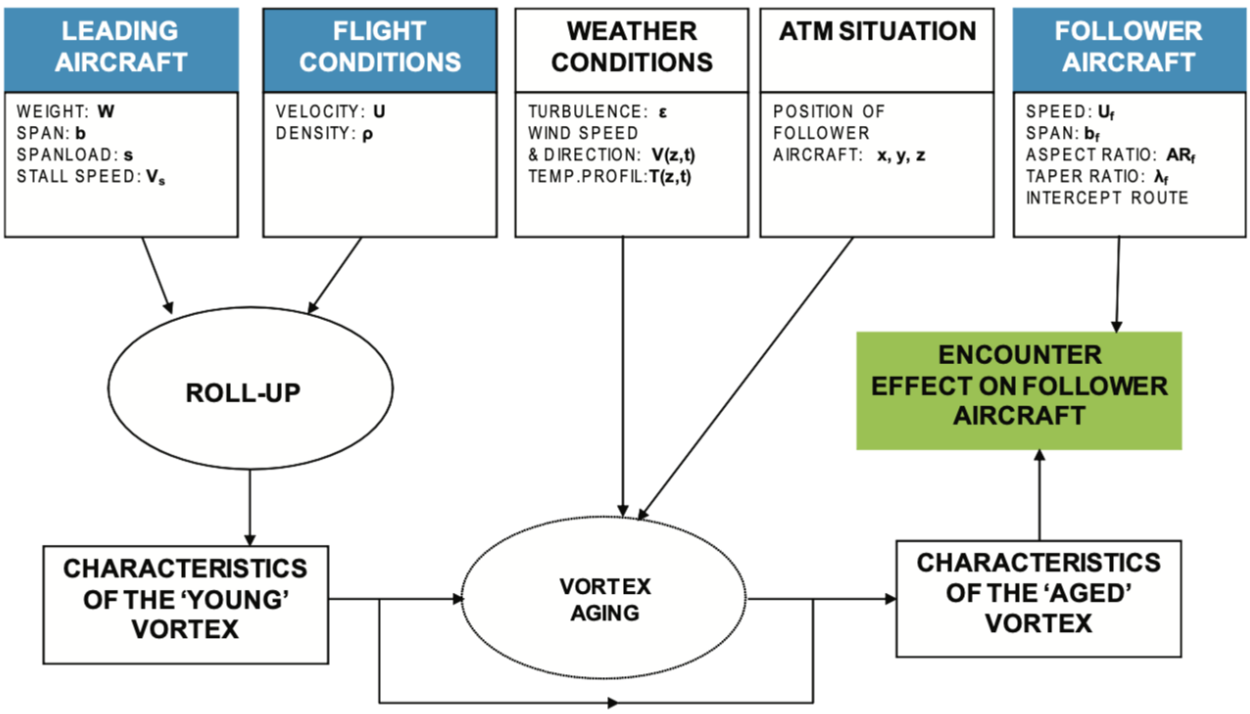

Figure 3.4 Factors affecting wake encounters (Liu 2007)

3.3 Wake Vortex Encounter Scenarios

Figure 3.5 shows three different vortex wake encounters in which a following aircraft flies through the vortex wake of a leading aircraft according to ICAO 1984 (page II-5-3-2), which is also visualized in De Kat 2007:

Scenario 1: The aircraft flies into the wake perpendicular to the vortex wake of an aircraft. This could cause high structural dynamic loads and increased turbulence during the wake vortex encounter.

Scenario 2: The aircraft flies parallel and between the trailing counter-rotating wing tip vortices. Due to the downwash in this region a wake encounter for a following aircraft can either reduce its rate of climb or increase its rate of descent, which can especially be a serious threat for aircraft during final approach.

Scenario 3: The aircraft flies along the vortex axis. This wake vortex encounter scenario is the most dangerous because the airplane flies into a velocity field which induces a roll moment on the following aircraft. This threat is especially of significance for aircraft flying in close proximity to the ground during approach in case the induced moment exceeds the roll control capability of the aircraft.

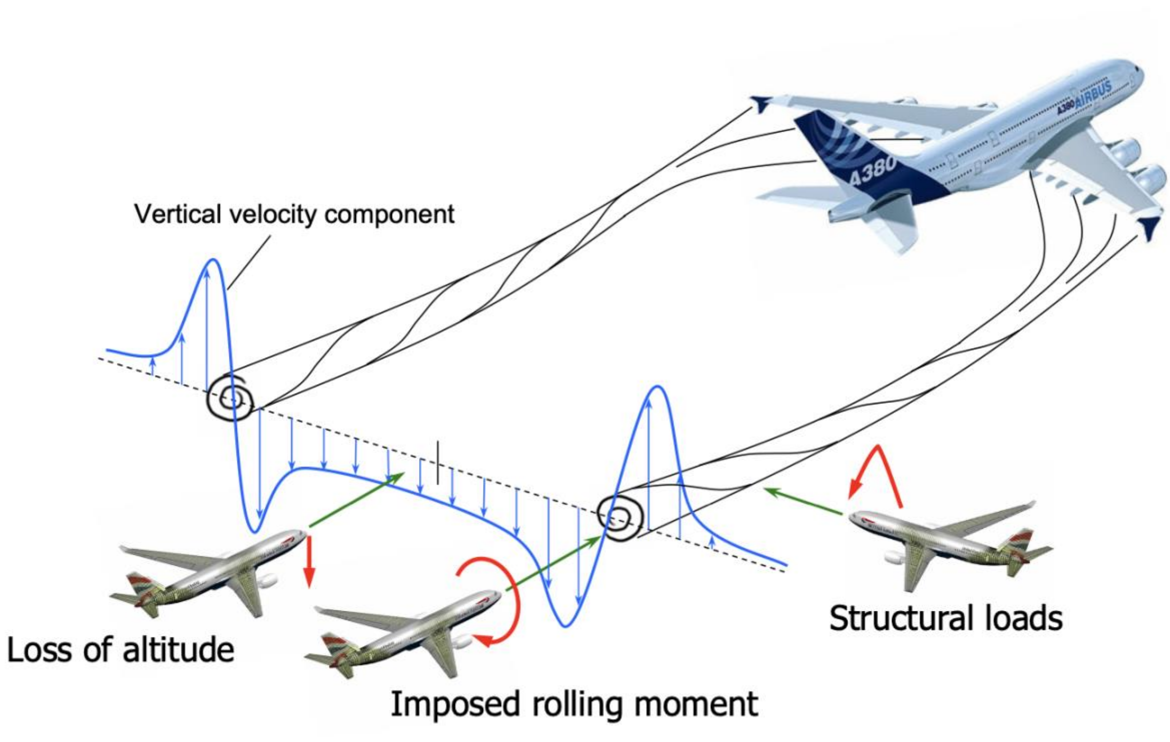

Figure 3.5 Three different vortex encounter scenarios (De Kat 2007)

3.4 Vortex Models

Several models are used to describe the velocity distribution in a wing tip vortex. Liu 2007 gives an overview of historical models and recent models that try to resemble measured velocity distributions. The Rankine vortex is the basic vortex model. The Lamb-Oseen vortex combines two vortices each similar to the Rankine vortex to a flow system as it is shed from the wing.

Rankine Vortex

The inner part of the vortex is in rotation like a solid body. At the center the flow is at rest. The rotational velocity is proportional to the radius. This holds true up to the core radius, r_c where the velocity, V is at its maximum. From here on the circulation, Γ is constant, and the velocity profile is reduced hyperbolically with $\frac{1}{r}$ .This vortex model has been used to describe wind velocities in a hurricane and is shown in Figure 3.6.

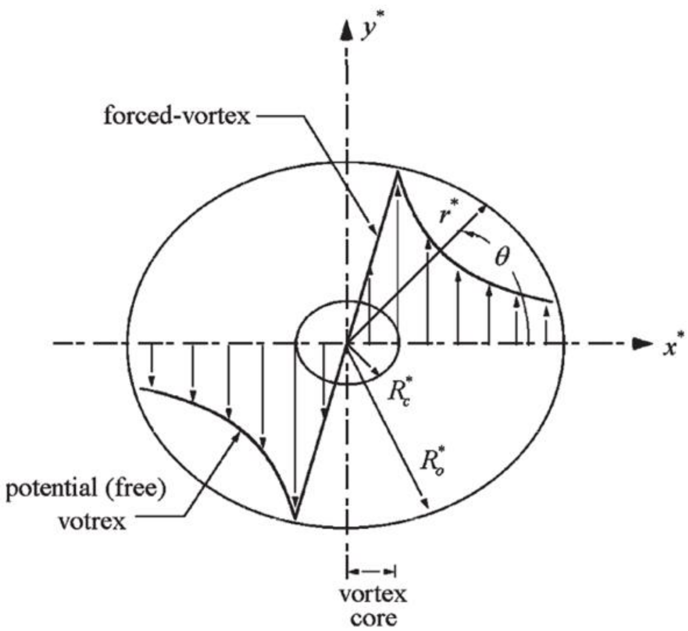

Figure 3.6 Schematic of the Rankine vortex velocity profile (Aboelkassem 2005)

Lamb-Oseen Vortex

Also, the Lamb-Oseen vortex has its inner part in rotation like a solid body. At the center the flow is at rest. The rotational velocity is proportional to the radius. At the core radius, r_c the velocity, V is at its maximum. From here on the velocity is reduced with increasing radius as given by

$$V_\theta(r) = \frac{\Gamma_\upsilon}{2\pi r} \cdot \left[1 - e^{-a \cdot \left(\frac{r}{r_c}\right)^2}\right] \tag{3.1}$$

with a = 1.256431, which puts the peak of velocity at the core radius, r_c. Figure 3.7 shows two counter-rotating Lamb-Oseen vortices of equal strength. The vortex cores are separated by the distance $b_0 = s \cdot b$ with $s = s_0 = \frac{\pi}{4}$ and b being the wing span. Hence the distance of the vortices is less than wing span. The circulation based on the elliptical loaded wing is given by

$$\Gamma_\upsilon = \frac{mg}{\rho s_0 b V} \tag{3.2}$$

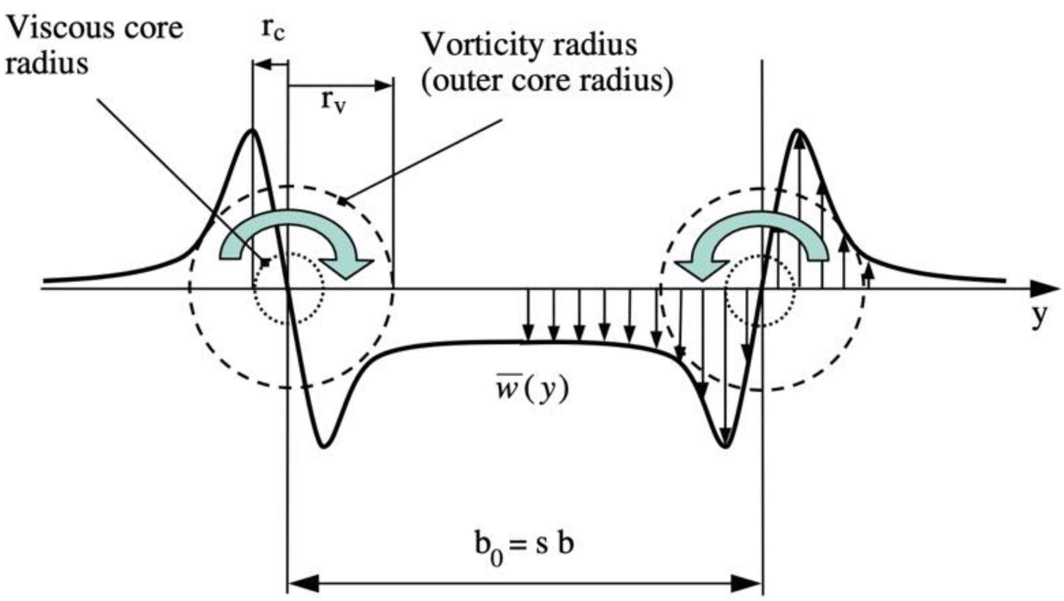

Figure 3.7 Superposition of two counter-rotating Lamb-Oseen vortices (Breitsamter 2010)

3.5 Wake Turbulence Classification

3.5.1 ICAO Categorization

The ICAO classifies wake turbulence based on the maximum take-off mass of the aircraft into the following wake turbulence categories according to ICAO 2016 (page 4-12):

- **J – SUPER**: Aircraft types with a maximum certificated take-off mass of 560000 kg
- **H – HEAVY**: Aircraft types with a maximum certificated take-off mass of less than 560000 kg but more than 136000 kg
- **M – MEDIUM**: Aircraft types with a maximum certificated take-off mass of less than 136000 kg but more than 7000 kg
- **L – LIGHT**: Aircraft types with a maximum certificated take-off mass of 7000 kg or less

Variants of an aircraft type with different take-off masses might be classified within different wake turbulence categories. Civil aviation authorities of individual states may also make further changes to the classification and, for example, introduce additional categories. ICAO 2022a contains designators for almost every aircraft. With ICAO 2022b it is possible to search for a specific aircraft and obtain the aircraft type designator and the WTC associated with it.

3.5.2 EUROCONTROL Categorization (RECAT-EU)

The European Organization for the Safety of Air Navigation, also known as Eurocontrol, has developed a re-categorization of the ICAO wake turbulence categorization, called "RECAT-EU" described in Eurocontrol 2018. In contrast to the ICAO categorization presented above, in this approach Eurocontrol also considers the wingspan. The aim of this re-categorization is to increase airport capacity by redefining wake turbulence categories and separation while adhering to safety standards. The criteria and rules for assigning wake turbulence categories according to Eurocontrol 2018 are presented in Figure 3.8.

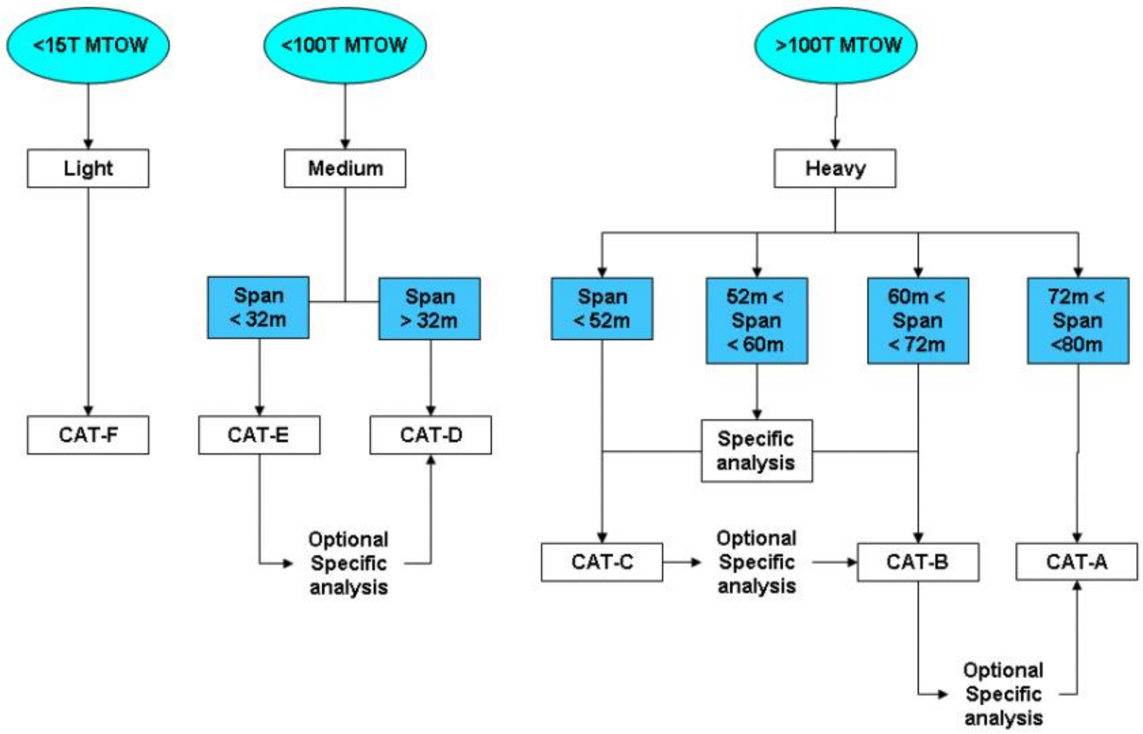

Figure 3.8 Wake turbulence categorization according to Eurocontrol (Eurocontrol 2018)

Eurocontrol uses categories from CAT-A to CAT-F. CAT-F (Light) is used for aircraft with a maximum certified take-off mass of less than 15000 kg. Aircraft with a take-off mass up to 100000 kg are classified in the medium category. If the wingspan is less than 32 m CAT-E (Lower Medium) is used. Otherwise, if the wingspan is larger than 32 m the aircraft is classified as CAT-D (Upper Medium). Aircraft with a take-off mass greater than 100000 kg are considered as heavy. If the wingspan is less than 52 m CAT-C (Lower Heavy) is used. For wingspans between 60 m and 72 m CAT-B (Upper Heavy) is applied. In case the wingspan is larger than 72 m the aircraft is classified as CAT-A (Super Heavy). Should the wingspan range between 52 m and 60 m either CAT-C or CAT-B is assigned depending on a further analysis.

Table 3.1 contains aircraft types assigned to wake turbulence categories classified by Eurocontrol.

Table 3.1 Aircraft types assigned to wake turbulence categories (Eurocontrol 2018)

Super Heavy	Upper Heavy	Lower Heavy	Upper Medium	Lower Medium	Light
CAT-A	CAT-B	CAT-C	CAT-D	CAT-E	CAT-F
A388	A332	A306	A318	AT43	FA10
A124	A333	A310	A319	AT45	FA20
	A343	B703	A320	AT72	D328
	A345	B752	A321	B712	E120
	A346	B753	AN12	B732	BE40
	A359	B762	B736	B733	H25B
	B744	B763	B737	B734	JS32
	B748	B764	B738	B735	JS41
	B772	C135	B739	CL60	LJ35
	B773	DC10	C130	CRJ1	LJ60
	B77L	DC85	IL18	CRJ2	SF34
	B77W	IL76	MD81	CRJ7	P180
	B788	MD11	MD82	CRJ9	C650
	B789		MD83	DH8D	C525
	IL96		MD87	E135	C180
			MD88	E145	C152
			MD90	E170	
			T204	E175	
				E190	
				E195	
				F70	
				F100	
				GLF4	
				RJ85	
				RJ1H	

3.5.3 FAA Categorization

The Federal Aviation Administration classifies wake turbulence in FAA 2019 by using the following categories mainly focusing on the maximum takeoff weight:

Category A – A388
Category B – Pairwise Upper Heavy aircraft
Category C – Pairwise Lower Heavy aircraft
Category D – Non-Pairwise Heavy aircraft
Category E – B757 aircraft
Category F – Upper Large aircraft excluding B757 aircraft
Category G – Lower Large aircraft
Category H – Upper Small aircraft with a maximum takeoff weight of more than 15400 pounds up to 41000 pounds
Category I - Lower Small aircraft with a maximum takeoff weight of 15400 pounds or less

Table 3.2 contains aircraft types assigned to wake turbulence categories classified by the Federal Aviation Administration according to FAA 2019.

Table 3.2 Aircraft types assigned to wake turbulence categories (FAA 2019)

Super	Upper Heavy	Lower Heavy	Non-Pairwise Heavy		B757	Upper Large		Lower Large		Upper Small	Lower Small
A	B	C	D		E	F		G		H	I
A388	A322	A306	A124	DC85	B752	A318	C130	AT43	E170	ASTR	BE10
	A333	A30B	A339	DC86	B753	A319	C30J	AT72	E45X	B190	BE20
	A343	A310	A342	DC87		A320	CVLT	CL60	E75L	BE40	BE58
	A345	B762	A3ST	E3CF		A321	DC93	CRJ1	E75S	B350	BE99
	A346	B763	A400	E3TF		B712	DC95	CRJ2	F16	C560	C208
	A359	B764	A50	E6		B721	DH8D	CRJ7	F18H	C56X	C210
	B742	C17	AN22	E767		B722	E190	CRJ9	F18S	C680	C25A
	B744	DC10	B1	IL62		B732	GL5T	CRJX	F900	C750	C25B
	B748	K35R	B2	IL76		B733	GLEX	DC91	FA7X	CL30	C402
	B772	MD11	B52	IL86		B734	GLF5	DH8A	GLF2	E120	C441
	B773		B703	IL96		B735	GLF6	DH8B	GLF3	F2TH	C525
	B77L		B741	K35E		B736	MD82	DH8C	GLF4	FA50	C550
	B77W		B743	KE3		B737	MD83	E135	SB20	GALX	P180
	B788		B74D	MYA4		B738	MD87	E145	SF34	H25B	PAY2
	B789		B74R	R135		B739	MD88			LJ31	PA31
	C5		B74S	T144			MD90			LJ35	PC12
	C5M		B78X	T160						LJ55	SR22
			BSCA	TU95						LJ60	SW3
			C135	VMT						SH36	
			C141							SW4	

The term pairwise in this context means according to FAA 2019 that “Each aircraft was addressed as both a leader and a follower in each pair”. Wake-based data was considered for the definition of FAA WTCs.

3.5.4 CAA Categorization

The Civil Aviation Authority (CAA), which is the British aviation authority, uses categories based on those of ICAO. The difference to ICAO is that there is the additional category S (Small), and the ICAO category M (Medium) is divided into UM (Upper Medium) and LM (Lower Medium). The following six categories apply for approach according to CAA 2022:

- **J – SUPER**: Only assigned to specific aircraft types: A388, A225, A124
- **H – HEAVY**: Aircraft types with a maximum certificated take-off mass of 136000 kg or more
- **UM – UPPER MEDIUM**: Aircraft types with a maximum certificated take-off mass of less than 136000 kg but more than 104000 kg
- **LM – LOWER MEDIUM**: Aircraft types with a maximum certificated take-off mass of 104000 kg or less but more than 40000 kg
- **S – SMALL:** Aircraft types with a maximum certificated take-off mass of 40000 kg or less but more than 17000 kg
- **L – LIGHT:** Aircraft types with a maximum certificated take-off mass of 17000 kg or less

3.6 Wake Vortex Separation

In ICAO 2016 and Eurocontrol 2018 the following separation minima presented in Table 3.3 based on the assigned wake turbulence category are defined.

Table 3.3 ICAO wake turbulence categories and separation minima (Eurocontrol 2018)

Aircraft categories		Separation minima
Leading aircraft	Following aircraft	
SUPER	HEAVY	6 NM
	MEDIUM	7 NM
	LIGHT	8 NM
HEAVY	HEAVY	4 NM
	MEDIUM	5 NM
	LIGHT	6 NM
MEDIUM	LIGHT	5 NM

Table 3.3 indicates that the WTC of the following aircraft is just as relevant as the WTC of the leading aircraft for the determination of separation minima. This can be explained by the fact that heavier aircraft are less at risk from wake vortices since they are more inert. Accordingly, in Figure 3.4, among the parameters of the follower aircraft, the aircraft mass is to be found missing.

In the context of RECAT-EU, in addition to new WTCs, new distance-based separation minima on approach and departure, shown in Table 3.4, were developed with the aim of improving airport capacity without compromising safety.

Table 3.4 RECAT-EU WT separation minima on approach and departure (Eurocontrol 2018)

Following aircraft / Leading aircraft		SUPER HEAVY CAT-A	UPPER HEAVY CAT-B	LOWER HEAVY CAT-C	UPPER MEDIUM CAT-D	LOWER MEDIUM CAT-E	LIGHT CAT-F
SUPER HEAVY	CAT-A	3 NM	4 NM	5 NM	5 NM	6 NM	8 NM
UPPER HEAVY	CAT-B		3 NM	4 NM	4 NM	5 NM	7 NM
LOWER HEAVY	CAT-C		2.5 NM	3 NM	3 NM	4 NM	6 NM
UPPER MEDIUM	CAT-D						5 NM
LOWER MEDIUM	CAT-E						4 NM
LIGHT	CAT-F						3NM

4 Methodology

As explained in Scholz 2018 when lift is generated, the wing presses the air it encounters in a downward direction. The air beyond the wingtips moves upward and then inward, which, together with the air flowing downward and then outward, results in the formation of two counter-rotating vortices.

Regardless of which vortex model from Section 3.4 is used, certain energy is required to generate wake vortices, which is represented in the induced drag of the aircraft. The induced power is hence the power induced into the wake of an airplane while generating lift. Consequently, lots of lift implies lots of induced power put into an aircraft's wake vortex. According to Anderson 1999 "the power needed to lift the airplane is proportional to the load (or weight) times the vertical velocity of the air". With increasing speed more air can be deflected downwards, decreasing the required power for lift. Furthermore, it can be concluded from the above-mentioned correlation that the required power for lift increases with higher mass. In the following, the equation for induced power is derived from induced drag (as a function of lift), and also from the energy in the vortex.

4.1 Induced Power Calculation

The approach used in this paper to categorize wake vortex strength according to Scholz 2022 considers the induced power contributed by the respective aircraft to its wake vortex. The induced power, P_{wake} results from the induced drag, D_i and the airspeed, V

$$P_{wake} = D_i \, V \tag{4.1}$$

The induced drag, D_i is calculated by using following formula:

$$D_i = \frac{1}{2} \rho \, V^2 \, C_{D_i} \, S \tag{4.2}$$

For the calculation of the induced drag the drag coefficient, C_{D_i} is required

$$C_{D_i} = \frac{{C_L}^2}{\pi \, A \, e} \tag{4.3}$$

By further transformations the lift coefficient is determined and then used in the previous formulas

$$m \, g = L = \frac{1}{2} \rho \, V^2 \, C_L \, S \tag{4.4}$$

$$C_L = \frac{2\, m\, g}{\rho\, V^2\, S} \tag{4.5}$$

The result is a formula for the calculation of the induced drag:

$$D_i = \frac{2\, m^2\, g^2}{\pi\, A\, e\, \rho\, V^2\, S} \tag{4.6}$$

By multiplication of the induced drag with the airspeed the following expression results for the induced power

$$P_{wake} = \frac{2\, g^2}{\pi} \frac{1}{b^2\, e} \frac{m^2}{\rho\, V} \tag{4.7}$$

The formula is split into three factors. The first factor contains constants, such as the gravitational acceleration, g. The second factor includes the wing span, b and the Oswald factor, e. The third factor consists of parameters, which are determined from flight operations: aircraft mass, m, approach speed, V and air density, ρ, which depends on the airfield altitude.

All parameters from Figure 3.4, which influence the roll-up of wake vortices are reflected in Equation 4.7. The span loading mentioned in Figure 3.4 is considered by using the Oswald factor as a correction factor for a non-elliptical span loading.

From the derived formula it becomes evident that with increasing aircraft mass the induced power increases. This may be explained by the fact that a larger mass requires more lift and consequently more induced power is contributed to the aircraft's wake. Simultaneously, as stated in Scholz 2018, the induced power decreases with increasing wing span and approach speed since by increasing the wing span, a larger mass of air can be affected using a smaller amount of speed to generate a certain amount of lift, resulting in less energy in the wake.

It is also possible to derive the induced power from the energy of Lamb-Oseen vortices shed from the wing. This is shown in Liu 2007.

$$P_{wake} = D_i\, V = E_k V \tag{4.8}$$

where E_k is the kinetic energy divided by the distance flown. Since energy or work is force times distance, the energy, E_k has the unit of force. E_k multiplied with the flight speed, V yields also induced power. The circulation based on the elliptical loaded wing is given by

$$\Gamma_v = \frac{mg}{\rho s_0 bV} \tag{4.9}$$

As a good approximation and under the assumption that the vorticity fields of the left and right vortex do not overlap, an approximation of the exact crossflow kinetic energy can be written as

$$E_k = \rho \frac{{\Gamma_v}^2}{2\pi} \left\{ \ln\left(\frac{s_0 b}{r_c}\right) + C \right\} \tag{4.10}$$

where C is a constant that depends only on the particular circulation profile. For the Lamb-Oseen vortices $C = 0.05617$. However, we obtain the value of the braced term as

$$\frac{(2s_0)^2}{e} \approx \ln\left(\frac{s_0 b}{r_{c,0}}\right) + C \tag{4.11}$$

with $s_0 = \frac{\pi}{4}$.

Substituting (4.11) in (4.10), inserting (4.9) and multiplying with V as in (4.8) yields induced power, P_{wake} as in (4.7).

The power in the fluid endangers an aircraft following behind in the axis of the vortex. The following aircraft experiences a rolling moment, L_R ,which causes an acceleration in roll, $\dot{p}$. The aircraft can counter the roll with aileron input, but if aileron authority is insufficient, the aircraft will continue to roll and bank. The aircraft's roll acceleration depends on its moment of inertia, I_x about the x-axis

$$\dot{p} = \frac{L_R}{I_x} \tag{4.12}$$

The rolling moment, L_R is proportional to air density, speed square, wing area, and span. The moment of inertia is roughly proportional to the aircraft mass and span square. After all, it is less clear how an aircraft will resist flying into a vortex. But rolling resistance will increase with aircraft wing loading, $\frac{m}{S}$ and span, b. Larger aircraft have clearly an advantage. Rolling resistance will decrease with aircraft speed, V and air density, ρ.

Aircraft wake turbulence categories (WTC) first of all group aircraft depending on their parameters generating a danger if flying ahead. The same WTCs are much less useful predicting rolling resistance of a following aircraft. Both characteristics are needed, if advice about aircraft separation is in question.

4.2 Estimation of the Oswald Factor

To calculate the induced power according to the equation shown in the preceding section, it is necessary to use the Oswald factor. In Nita 2012 two methods for estimating the Oswald factor are presented, which are described in the following.

4.2.1 Calculation of the Oswald Factor without Input of C_{D0}

The equation to calculate the Oswald Factor without using the zero drag coefficient is:

$$e = e_{theo} \cdot k_{e,F} \cdot k_{e,D_0} \cdot k_{e,M} \cdot k_{e,WL} \tag{4.13}$$

The correction factor, $k_{e,WL}$ is only used for aircraft with winglets and is calculated with following equation:

$$k_{e,WL} = \left(1 + \frac{2}{k_{WL}} \frac{h}{b}\right)^2 \tag{4.14}$$

h is the winglet height and for k_{WL} the average value of 2,83 can be used.

k_{e,D_0} is a correction factor which considers the viscous drag due to lift and depends on the aircraft category. Different values for this correction factor are shown in Table 4.1.

Table 4.1 Values for the correction factor *k_e_D0* (Scholz 2012)

Aircraft category	k_{e,D_0}
Jet	0,873
Business Jet	0,864
Turboprop	0,804
General Aviation	0,804

$k_{e,F}$ is a correction factor which considers the losses due to the fuselage and is calculated with following equation:

$$k_{e,F} = 1 - 2\left(\frac{d_F}{b}\right)^2 \tag{4.15}$$

d_F is the diameter of the fuselage, $\frac{d_F}{b}$ is the ratio of the fuselage diameter and the wingspan.

$k_{e,M}$ is a correction factor which considers compressibility effects on induced drag. Since this thesis only considers the Mach numbers of aircraft on approach, and they are below the compressibility Mach number, this factor for estimating the Oswald factors is not considered further.

e_{theo} is the theoretical Oswald factor which can be calculated for unswept wings with the following equations:

$$e_{theo} = \frac{1}{1 + f(\lambda - \Delta\lambda) \cdot A} \tag{4.16}$$

with

$$\Delta\lambda = -0{,}357 + 0{,}45 \cdot e^{-0{,}0375 \cdot \varphi_{25}} \tag{4.17}$$

and

$$f(\lambda - \Delta\lambda) = 0{,}0524(\lambda - \Delta\lambda)^4 - 0{,}15(\lambda - \Delta\lambda)^3 + 0{,}1659(\lambda - \Delta\lambda)^2 - 0{,}0706(\lambda - \Delta\lambda) + 0{,}011 \tag{4.18}$$

λ is the taper ratio, A is the Aspect ratio and φ_{25} is the sweep angle in degrees measured at a quarter of the chord length.

4.2.2 Calculation of the Oswald Factor with Input of C_{D0}

The equation to calculate the Oswald Factor with using the zero drag coefficient is as follows:

$$e = \frac{k_{e,M}}{Q + P\pi A} \tag{4.19}$$

with

$$Q = \frac{1}{e_{theo} \cdot k_{e,F}} \tag{4.20}$$

and

$$P = 0{,}38 \cdot C_{D,0} \tag{4.21}$$

As mentioned in the previous section $k_{e,M}$ is not considered due to the low approach speeds, therefore the value of 1 is assumed for $k_{e,M}$. The theoretical Oswald factor, e_{theo} and the correction factor, $k_{e,F}$ are used from the previous calculation.

The zero drag coefficient is calculated according to Scholz 2015 with following equation:

$$C_{D,0} = C_{fe} \cdot \frac{S_{wet}}{S_W} \tag{4.22}$$

with $C_{fe} = 0{,}003$. S_{wet} is the wetted aircraft area and S_W is the reference wing area. Both values are used from Schlueter 2006.

Due to the relatively high effort to calculate the wetted area, the Oswald factors are calculated using the second method for only 12 of the total 89 aircraft considered. The comparison of the Oswald factors from both methods shows no significant deviation.

4.3 Aircraft Selection

A total of 89 different aircraft models are used for the calculation of the induced power. The selected airplane models differ significantly in wingspan, airplane mass, approach speed, which are the parameters required for the calculation of the induced power.

The selection of aircraft is based on the Eurocontrol categorization. All aircraft that are listed in the Eurocontrol categorization in Section 3.5.2 are examined. Some of these aircraft are not included in the FAA categorization. Instead, the FAA categorization contains other aircraft that are not included in the Eurocontrol categorization. These were not considered for the calculation, as the Eurocontrol categorization contains sufficient different aircraft which significantly differ from each other. For all aircraft from Table 4.2, the CAA and ICAO provide a WTC depending on the aircraft mass which can be found using ICAO 2022b (for ICAO WTC). The order in which the aircraft are listed corresponds to the one used by Eurocontrol.

Table 4.2 Examined aircraft models

Aircraft model	Type Designator	Aircraft model	Type Designator
Airbus A-380-800	A388	McDonnell Douglas MD-88	MD88
Antonov An-124	A124	McDonnell Douglas MD-90	MD90
Airbus A-330-200	A332	Tupolev Tu-204	T204
Airbus A-330-300	A333	ATR-42-300	AT43
Airbus A-340-300	A343	ATR-42-500	AT45

Cont.: Table 4.2 Examined aircraft models

Aircraft model	Type Designator	Aircraft model	Type Designator
Airbus A-340-500	A345	ATR-72	AT72
Airbus A-340-600	A346	Boeing 717-200	B712
Airbus A-350-900 XWB	A359	Boeing 737-200	B732
Boeing 747-400	B744	Boeing 737-300	B733
Boeing 747-8	B748	Boeing 737-400	B734
Boeing 777-300	773	Bombardier Challenger 650	CL60
Boeing 777-200LR	B77L	Canadair CRJ-100	CRJ1
Boeing 777-300ER	B77W	Canadair CRJ-200	CRJ2
Boeing 787-8	B788	Canadair CRJ-700	CRJ7
Boeing 787-9	B789	Canadair CRJ-900	CRJ9
Ilyushin Il-96-300	IL96	De Havilland DHC-8 Q400	DH8D
Airbus A-300-600	A306	Embraer ERJ-135	E135
Airbus A-310	A310	Embraer ERJ-145	E145
Boeing 707-320B	B703	Embraer ERJ-170	E170
Boeing 757-200	B752	Embraer ERJ-175	E175
Boeing 757-300	B753	Embraer ERJ-190	E190
Boeing 767-200	B762	Embraer ERJ-195	E195
Boeing 767-300	B763	Fokker 70	F70
Boeing 767-400ER	B764	Fokker 100	F100
Boeing C-135	C135	Gulfstream 4	GLF4
McDonnell Douglas DC-10-30	DC10	Avro RJ-85	RJ85
Douglas DC-8-50	DC85	Avro RJ-100	RJ1H
Ilyushin Il-76	IL76	Dassault Falcon 10	FA10
McDonnell Douglas MD-11	MD11	Dassault Falcon 20	FA20
Airbus A-318	A318	Dornier 328	D328
Airbus A-319	A319	Embraer EMB-120	E120
Airbus A-320	A320	Beechcraft Beechjet 400A	BE40
Airbus A-321	A321	Raytheon Hawker 800	H25B
Antonov An-12	AN12	BAe 32	JS32
Boeing 737-600	B736	BAe 41	JS41
Boeing 737-700	B737	Learjet 35	LJ35
Boeing 737-800	B738	Learjet 60	LJ60
Boeing 737-900	B739	Saab 340	SF34
Lockheed C-130J	C130	Piaggio P-180 Avanti	P180
Ilyushin Il-18	IL18	Cessna 650	C650
McDonnell Douglas MD-81	MD81	Cessna 525	C525
McDonnell Douglas MD-82	MD82	Cessna 180	C180
McDonnell Douglas MD-83	MD83	Cessna 152	C152
McDonnell Douglas MD-87	MD87		

5 Results

5.1 Recommended WTC Classification

The equation derived in Section 4.1 is used to calculate the induced power of 89 different aircraft models. The result is presented in Figure 5.1.

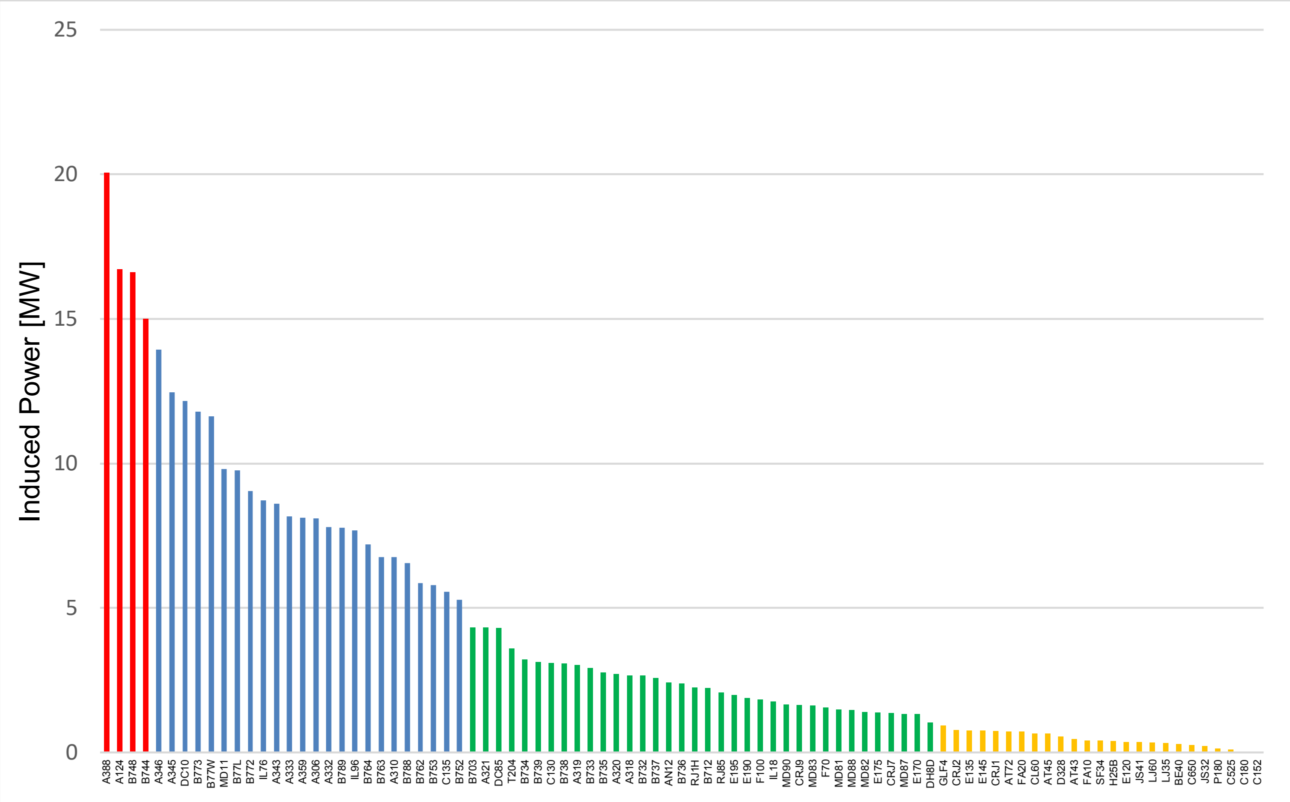

Figure 5.1 Examined aircraft sorted according to induced power in descending order

The examined aircraft have been sorted in descending order according to the induced power they respectively contribute to their wake vortices. Based on the results of this calculation, the following "HAW Hamburg Wake Turbulence Categories" (HAW Hamburg WTC) listed in Table 5.1 are proposed.

Following ICAO and to avoid complexity, four different categories have been defined. The lowest WTC contains mainly aircraft from business and general aviation. For the definition of CAT II and CAT III, the distinction between narrow body and wide body aircraft is used as a reference. For the lower threshold of CAT I, the induced power value of 15 MW for the B744 has proven to be a clearly identifiable limit. The different wake turbulence categories are indicated using different colors in Figure 5.1.

Table 5.1 HAW Hamburg Wake Turbulence Categories

HAW Hamburg WTC	Induced Power [MW]
CAT I	> 15
CAT II	5 – 15
CAT III	1 – 5
CAT IV	< 1

The categorization of the aircraft from Table 4.2 according to the HAW Hamburg WTC results as given in Table 5.2.

Table 5.2 Aircraft types assigned according to HAW Hamburg WTC

CAT I	CAT II	CAT III	CAT IV
A388	A346	B703	GLF4
A124	A345	A321	CRJ2
B748	DC10	DC85	E135
B744	B773	T204	E145
	B77W	B734	CRJ1
	MD11	B739	AT72
	B77L	C130	FA20
	B772	B738	CL60
	IL76	A319	AT45
	A343	B733	D328
	A333	B735	AT43
	A359	A320	FA10
	A306	A318	SF34
	A332	B737	H25B
	B789	AN12	E120
	IL96	B736	JS41
	B764	B712	LJ60
	B763	RJ85	LJ35
	A310	E195	BE40
	B788	E190	C650
	B762	F100	JS32
	B753	IL18	P180
	C135	MD90	C525
	B752	CRJ9	C180
		MD83	C152
		F70	
		MD81	
		MD88	
		MD82	
		E175	
		CRJ7	
		MD87	

5.2 Comparison with Conventional Classification

In Figure 5.2 to Figure 5.6 the wake turbulence classification is indicated with a dot versus the calculated induced power of each aircraft from Table 4.2. Figure 5.2 shows the HAW Hamburg WTC. Since they are defined by induced power, the dots jump in clear steps with increasing induced power.

In contrast to HAW Hamburg WTC the ICAO, FAA, CAA and Eurocontrol wake turbulence categorization occasionally assign a smaller WTC to an aircraft with larger induced power. This is indicated by an overlap of categories when plotted against induced power. Most inconsistency (and thus the most overlaps) is in the categorization of the FAA. With regard to the Eurocontrol categorization the main inconsistency is found between CAT-B and CAT-C. When categorizing Wake Turbulence, Eurocontrol also considers wing span. Aircraft with larger wing span are assigned to higher WTC. This is in contradiction to the fact that the induced power decreases with increasing wing span and thus the aircraft would have to be classified in a lower WTC.

For the ICAO categorization, the greatest overlap exists between the wake turbulence categories H (Heavy) and M (Medium). Regarding the CAA categorization the greatest overlap is visible between the categories H (Heavy) and UM (Upper Medium) and between LM (Lower Medium) and S (Small).

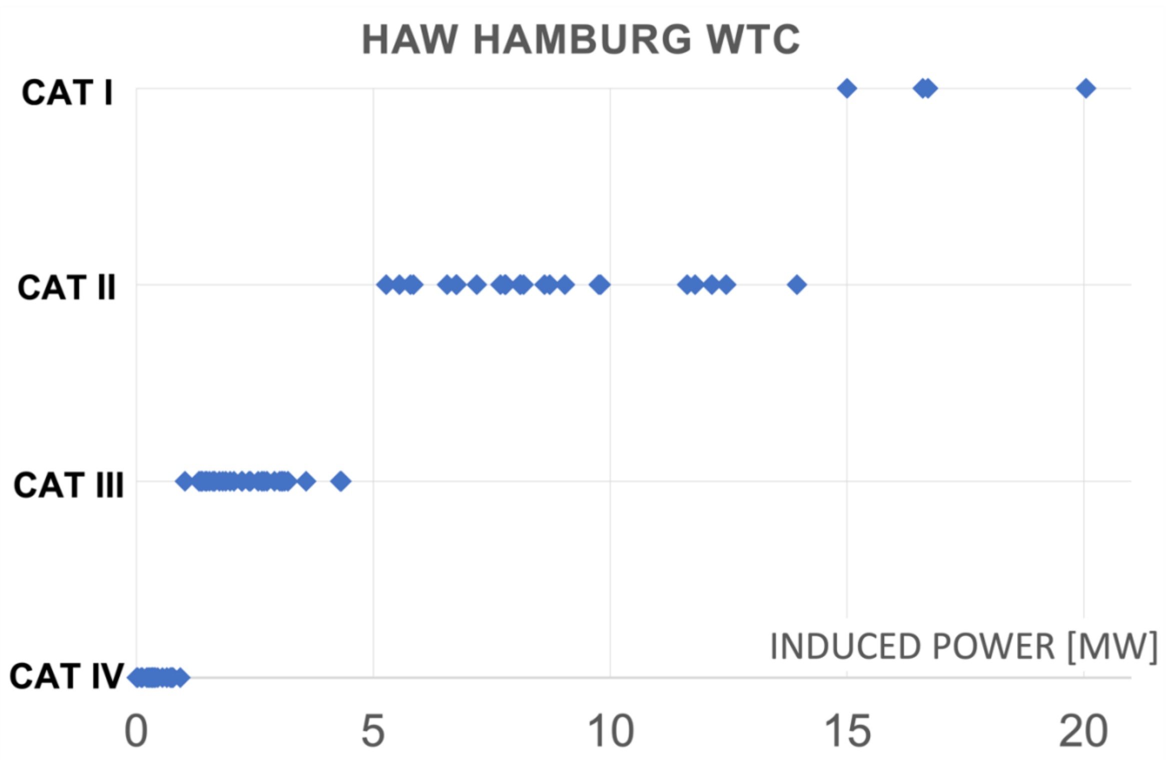

Figure 5.2 Induced power according HAW Hamburg WTC

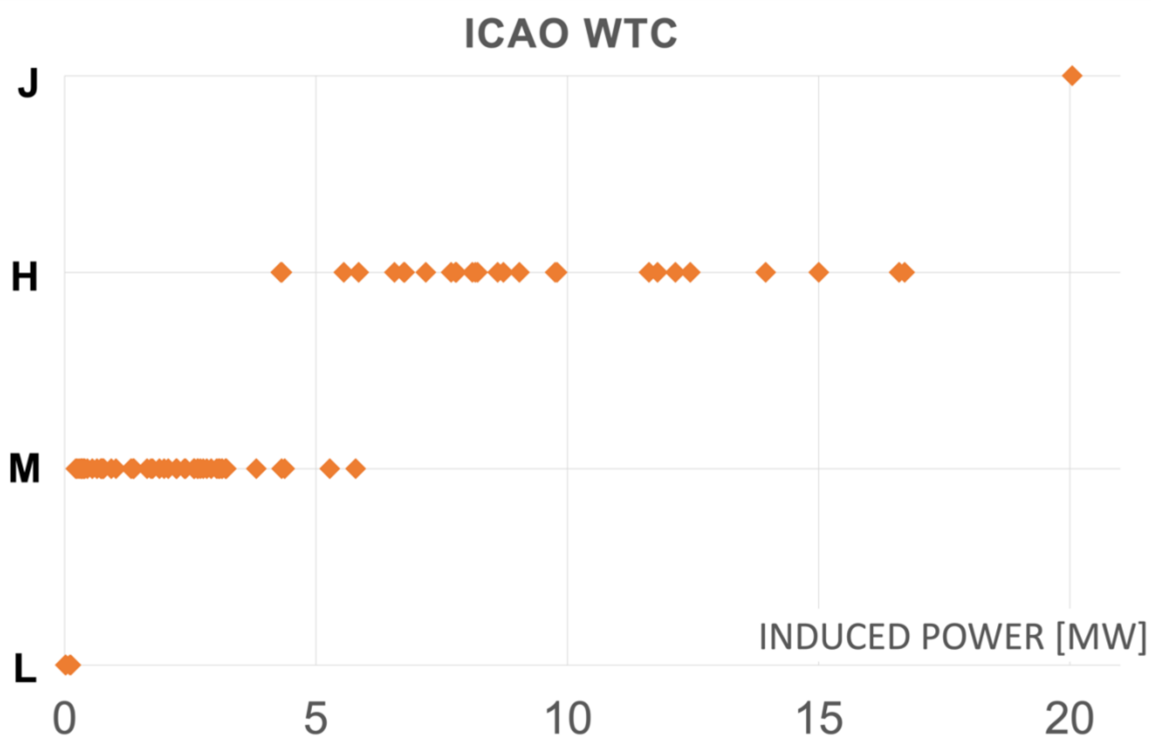

Figure 5.3 Induced power according ICAO WTC

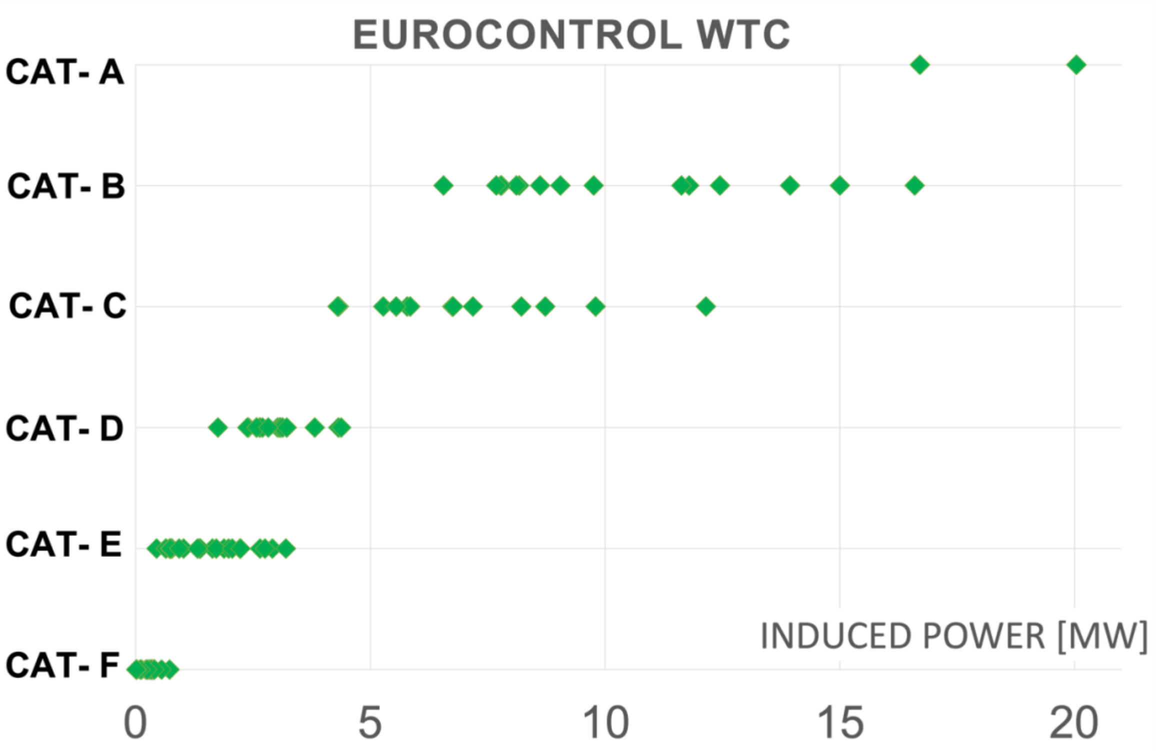

Figure 5.4 Induced power according EUROCONTROL WTC

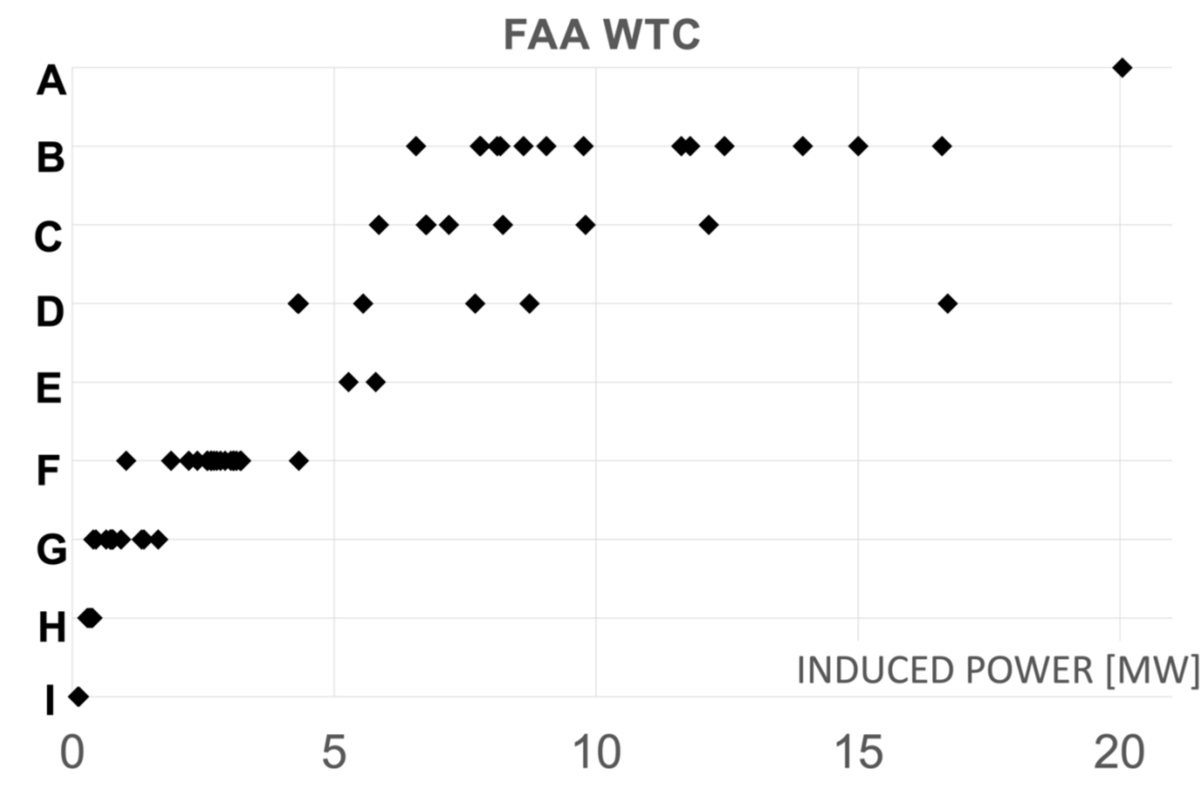

Figure 5.5 Induced power according FAA WTC

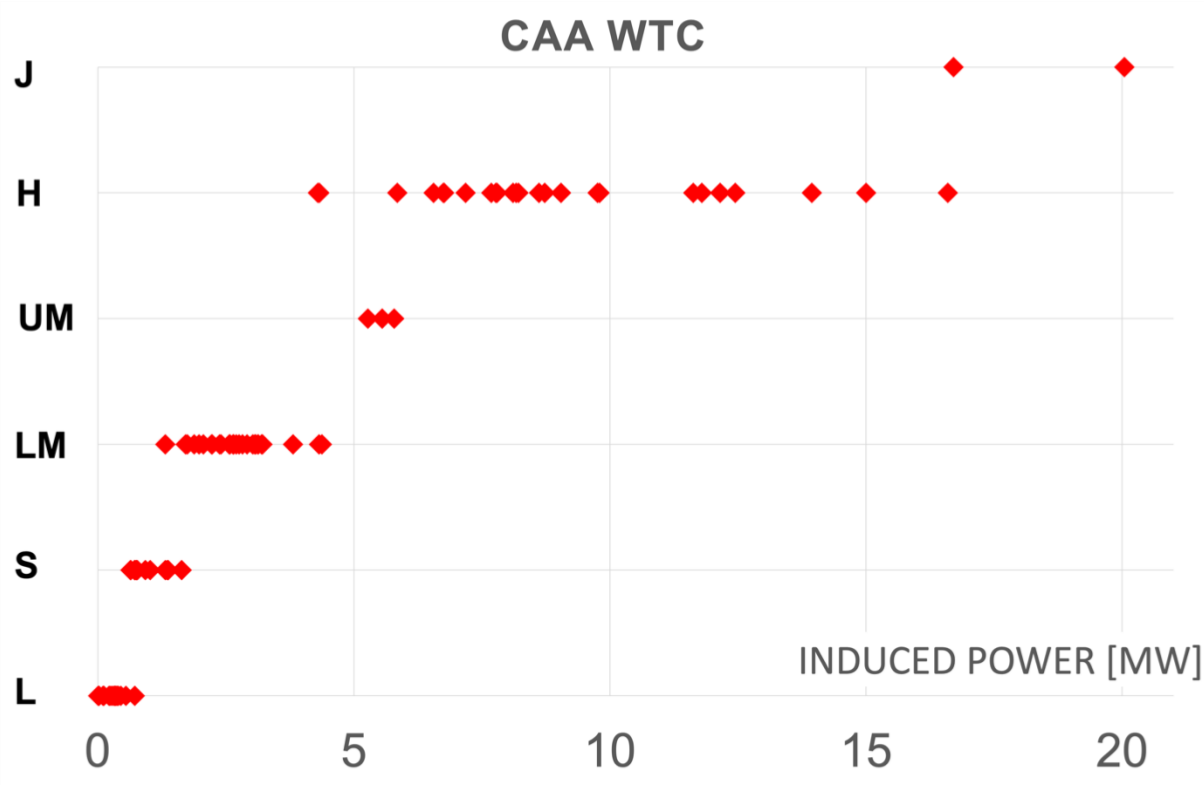

Figure 5.6 Induced power according CAA WTC

5.3 Evaluation of A380 and B757 WTC

In Section 2 it is mentioned that ICAO created a separate WTC for the A380 due to its large mass. As derived in Section 4.1 the aircraft mass has the greatest influence on the induced power, evident by the fact that the mass is squared.

Considering the results of the induced power calculation presented in Figure 5.1, the decision of ICAO to introduce a new WTC for the A380 can be agreed with, since the significantly higher mass causes a considerably larger induced power compared to all other examined aircraft.

Another aspect mentioned in Section 2 is the categorization of B757 aircraft. According to the ICAO classification the B757 is assigned to the WTC Medium. Nevertheless, some states apply a higher WTC to the B757.

With regard to the results in Section 5.1, it is evident that the B757 is assigned to the second-highest WTC and is thus classified higher than other narrowbody aircraft. In this respect, from the perspective of induced power, the decision of some countries to apply the WTC Heavy to B757 aircraft is justified.

6 Summary and Conclusions

The objective of this thesis was to define new Wake Turbulence Categories based on induced power calculation and compare them to the categories which are used by Eurocontrol, FAA, CAA, and the ICAO to classify wake turbulence.

The literature review has shown that much research has been done on the subject of wake turbulence, hence today there is a lot of knowledge about it. Nevertheless, the classification of wake turbulence is still rather rudimentary. Induced power was considered as the relevant factor for the categorization of aircraft into WTC, since it describes how much energy per unit of time is induced into the wake of an aircraft when generating lift.

The calculation of the induced power for the different aircraft models resulted in four Wake Turbulence Categories: For an induced power greater than 15 MW the highest category CAT I is assigned. CAT II is used for aircraft with an induced power ranging from 5 to 15 MW. If the induced power is between 1 and 5 MW the aircraft is assigned to CAT III. The lowest category CAT IV is assigned to aircraft with induced powers smaller than 1 MW.

The comparison to conventional wake turbulence classification systems showed that ICAO, FAA, CAA and Eurocontrol frequently assign smaller WTC to aircraft with larger induced powers. In contrast, the recommended categories are based on a clear assignment according to the induced power calculation.

Regarding the categorization of the A380, it has been shown that the definition of the WTC Super by ICAO is correct. It has also been proven that the B757 is rightly assigned to the WTC Heavy by some states.

The impact and different wake encounter scenarios for aircraft flying into the wake of a leading aircraft was presented in Section 3. The greater the induced power an aircraft contributes to its wake vortex, the more hazardous the wake encounter is for following aircraft. Therefore, and to conclude this thesis the recommended HAW Hamburg WTC should be used instead of the established WTC to categorize Wake Turbulence.

7 Recommendations

In this thesis, the minimum separation distances have not been examined nor the extent to which the consideration of induced power may reduce minimum separation distances. Physics based separation minima would need a double classification of each aircraft: a) classification related to wake vortex generation as done in this thesis and b) classification related to rolling resistance. The wake separation minima would then be allocated from a pairwise comparison.

Also, the idea of a division into six different categories analogous to RECAT-EU could be discussed. The limits for the different categories could be based on the categories proposed by RECAT-EU. Thus, RECAT-EU could be referred to when considering the optimization of separation minima. In Eurocontrol 2018 it is mentioned that the proposed re-categorization optimization of separation minima is not based on calculations, but on “structured arguments with supporting evidence“. Hence, the consideration of induced power, presented in the context of this thesis, for the evaluation of wake turbulence, could be used as a convincing argument.

List of References

ABOELKASSEM, Yasser, VATISTAS, Georgios, ESMAIL, Nabil, 2005. Viscous Dissipation of Rankine Vortex Profile in Zero Meridional Flow. In: *Acta Mechanica Sinica*, vol. 21, no. 6, pp. 550-556.
Available from: https://doi.org/10.1007/s10409-005-0073-3 (Closed Access)
Open Access at: https://bit.ly/3FUDMt6
Archived at: https://perma.cc/WN5J-QYDS

ANDERSON, David, EBERHARDT, Scott, 1999. How Airplanes Fly: A Physical Description of Lift. In: *Sport Aviation.*
Available from: https://bit.ly/3jB3lrE
Archived at: https://perma.cc/TDD7-C24V

BIENIEK, David, LUCKNER, Robert, 2007. Parametric Study & Simplified Approach to Wake Vortex Encounter Offline Simulation. In: *European Air and Space Conference* (Berlin, 10. - 13. September 2007).
Available from: https://bit.ly/3I00rqQ
Archived at: https://perma.cc/5CWW-M3XW

BREITSAMTER, Christian, 2010. Wake Vortex Characteristics of Transport Aircraft. In: *Progress in Aerospace Sciences*, vol. 47, no. 2, pp. 89-134.
Available from: https://doi.org/10.1016/j.paerosci.2010.09.002 (Closed Access)

CIVIL AVIATION AUTHORITY, 2022. *Manual of Air Traffic Services – Part 1.*
Available from: https://bit.ly/3hEd0xj
Archived at: https://perma.cc/83BA-K3D4

DE KAT, Roeland, 2007. *Vortex Decay behind a Generic Wing-Flap-Jet Aircraft Model: A Time Dependent Vortex Model.* Master Thesis. Delft: Delft University of Technology.
Available from: https://bit.ly/3FGsd95
Archived at: https://perma.cc/JT35-ESTL

FEDERAL AVIATION ADMINISTRATION, 2019. *Consolidated Wake Turbulence (CWT) Separation Standards.*
Available from: https://bit.ly/3W9b0Md
Archived at: https://perma.cc/U97N-BSYY

GERZ, Thomas, et al., 2009. The Wake Vortex Prediction and Monitoring System WSVBS Part II: Performance and ATC Integration at Frankfurt Airport. In: *Air Traffic Control Quarterly,* vol. 17, no. 4, pp. 323-346.
Available from: https://elib.dlr.de/61401

HOLZÄPFEL, Frank, GERZ, Thomas, BAUMANN, Robert, 2001. The Turbulent Decay of Trailing Vortex Pairs in Stably Stratified Environments. In: *Aerospace Science and Technology*, vol. 5, no. 2, pp. 95-108.
Available from: https://doi.org/10.1016/S1270-9638(00)01090-7 (Closed Access)
Open Access at: http://www.pa.op.dlr.de/wirbelschleppe/publ/AST2001.pdf
Archived at: https://perma.cc/RJ7J-K77H

HOLZÄPFEL, Frank, et al., 2003a. Strategies for Circulation Evaluation of Aircraft Wake Vortices Measured by Lidar. In: *Journal of Atmospheric and Oceanic Technology*, vol. 20, no. 8, pp. 1183-1195.
Available from: https://doi.org/10.1175/1520-0426(2003)020<1183:SFCEOA>2.0.CO;2

HOLZÄPFEL, Frank, 2003b. Probabilistic Two-Phase Wake Vortex Decay and Transport Model. In: *Journal of Aircraft*, vol. 40, no. 2, pp. 323-331.
Available from: https://doi.org/10.2514/2.3096 (Closed Access)
Open Access at: http://www.pa.op.dlr.de/wirbelschleppe/publ/JoA2003.pdf
Archived at: https://perma.cc/3UF3-PQNH

HOLZÄPFEL, Frank, et al., 2003c. Analysis of Wake Vortex Decay Mechanisms in the Atmosphere. In: *Aerospace Science and Technology*, vol. 7, no. 5, pp. 263-275.
Available from: https://doi.org/10.1016/S1270-9638(03)00026-9 (Closed Access)
Open Access at: http://www.pa.op.dlr.de/wirbelschleppe/publ/AST2003.pdf
Archived at: https://perma.cc/5249-ZL2C

HOLZÄPFEL, Frank, et al., 2009. The Wake Vortex Prediction and Monitoring System WSVBS Part I: Design. In: *Air Traffic Control Quartley,* vol. 17, no. 4.
Available from: https://doi.org/10.2514/atcq.17.4.301 (Closed Access)
Open Access at: https://elib.dlr.de/61403

INTERNATIONAL CIVIL AVIATION ORGANIZATION, 1984. *Air Traffic Services Planning Manual (Doc 9426-AN/924).* Montréal.
Available from: https://bit.ly/3WThorh
Archived at: https://perma.cc/DNR6-XB7D

INTERNATIONAL CIVIL AVIATION ORGANIZATION, 2016. *Doc 4444, Procedures for Air Navigation Services — Air Traffic Management.* Montéal.
Available from: https://bit.ly/3VfrOjG
Archived at: https://perma.cc/843P-A34A

INTERNATIONAL CIVIL AVIATION ORGANIZATION, 2022a. *Doc 8643, Aircraft Type Designators*. Montéal.
Available from: https://bit.ly/3WNxqTd
Archived at: https://perma.cc/392N-8FBC

INTERNATIONAL CIVIL AVIATION ORGANIZATION, 2022b. DOC 8643 - Aircraft Type Designators.
Available from: https://www.icao.int/publications/DOC8643/Pages/Search.aspx

LIU, Chao, 2007. *Wake Vortex Encounter Analysis with Different Wake Vortex Models Using Vortex-Lattice Method.* Master Thesis. Delft: Delft University of Technology.
Available from: https://bit.ly/3WtcCjH
Archived at: https://perma.cc/HX9C-JY94

LIU, Xiaoying, et al., 2021. Observation of Aircraft Wake Vortex Evolution under Crosswind Conditions by Pulsed Coherent Doppler Lidar. In: *Atmosphere*, vol. 12, art. 49.
Available from: https://doi.org/10.3390/atmos12010049

LONGMAN, 2022a. Comparison.
Available from: https://www.ldoceonline.com/dictionary/comparison

LONGMAN, 2022b. Aircraft.
Available from: https://www.ldoceonline.com/dictionary/aircraft

LONGMAN, 2022c. Calculation.
Available from: https://www.ldoceonline.com/dictionary/calculation

MCLEAN, Doug, 2005. *Wingtip Devices: What They Do and How They Do It.* Performance and Flight Operations Engineering Conference, Boeing, Article 4.
Available from: https://bit.ly/3VfLmnU
Archived at: https://perma.cc/NKU7-TRZG

MERRIAM-WEBSTER, 2022. Category.
Available from: https://www.merriam-webster.com/dictionary/category

NIŢĂ, Mihaela, SCHOLZ, Dieter, 2012. *Estimating the Oswald Factor from Basic Aircraft Geometrical Parameters.* In: Publikationen zum DLRK 2012 (Deutscher Luft- und Raumfahrtkongress, Berlin, 10. - 12. September 2012).
Available from: https://nbn-resolving.org/urn:nbn:de:101:1-201212176728
Archived at: https://perma.cc/KTR4-RU3H

PAN, Weijun, WANG, Jingkai, XU, Yaxing, 2022. Research on Optimization of Wake Safety Interval for Domestic ARJ21 Aircraft during Take-Off and Landing. In: *2022 3rd Asia-Pacific Conference on Image Processing, Electronics (IPEC'22)* (Dalian, 14. - 16. April 2022)
Available from: https://doi.org/10.1145/3544109.3544124 (Closed Access)

RILL, Stefan, 1996. Einleitung: Abwind und induzierter Widerstand. In: *Aerodynamik des Flugzeugs.* Hochschule Bremen.
Available from: https://bit.ly/3hB8TlB
Archived at: https://perma.cc/5CZY-2WG8

ROBINS, Robert, DELISI, Donald, 2002. *NWRA AVOSS Wake Vortex Prediction Algorithm Version 3.1.1.* Langley Research Center. Bellevue, Washington.
Available from: https://ntrs.nasa.gov/citations/20020060722

ROOSELEER, Frederic, TREVE, Vincent, 2018. *"RECAT-EU" European Wake Turbulence Categorisation and Separation Minima on Approach and Departure.* EUROCONTROL. Brussels, Belgium.
Available from: https://bit.ly/3VcoDt1
Archived at: https://perma.cc/44U3-86X2

ROSSOW, Vernon, 1999. Lift-Generated Vortex Wakes of Subsonic Transport Aircraft. In: *Progress in Aerospace Sciences,* vol. 35, no. 6, pp. 507-660.
Available from: https://doi.org/10.1016/S0376-0421(99)00006-8 (Closed Access)

SCHLÜTER, Andre John, 2006. *Maximale Gleitzahl, Streckung und Benetzte Fläche.* Project. Hamburg: Hamburg University of Applied Sciences.
Available from: https://bit.ly/3v19m3l
Archived at: https://perma.cc/3JNY-77VE

SCHOLZ, Dieter, 2015. Drag Prediction. In: *Aircraft Design.* Hamburg Open Online University.
Available from: http://hoou.ProfScholz.de
Archived at: https://perma.cc/Y8CK-XNW6

SCHOLZ, Dieter, 2018. Definition and Discussion of the Intrinsic Efficiency of Winglets. In: *INCAS BULLETIN*, vol. 10, 1/2018, pp. 117-134.
Available from: https://doi.org/10.13111/2066-8201.2018.10.1.12
Archived at: https://perma.cc/SJF6-K7AB

SCHOLZ, Dieter, 2022. *Airbus A380 - Ein Nachruf.* Report. Hamburg: Hamburg University of Applied Sciences, Aircraft Design and Systems Group (AERO).
Available from: https://doi.org/10.48441/4427.402
Archived at: https://perma.cc/PE7T-MXMP

SKYBRARY. 2022a. ICAO Wake Turbulence Category.
Available from: https://bit.ly/3BObC1S
Archived at: https://perma.cc/49PU-HJV9

SKYBRARY. 2022b. Wake Vortex Turbulence.
Available from: https://bit.ly/3G3We3N
Archived at: https://perma.cc/W9L6-4FDR

SPEIJKER, Lennaert, et al., 2007. ATC-Wake: Integrated Wake Vortex Safety and Capacity System. In: *Journal of Air Traffic Control*, vol. 49, no. 1, pp. 17-32.
Available from: https://bit.ly/3FWbvCM
Archived at: https://perma.cc/46NJ-VHMH

All online resources have been accessed on 23.12.2022 or later.

Appendix A – Induced Power Calculation

Index	Type Designator	Model	WTC (EC)	WTC (ICAO)	WTC (FAA)	WTC (CAA)	max. landing weight [kg]	wing span [m]	approach speed (VAT) [m/s]	Oswald Factor [-]	Induced Power [W]	Induced Power [MW]
1	A388	Airbus A-380-800	CAT-A	J	A	J	394000	79,75	72,01646091	0,845065	20044459,8	20,04445982
2	A124	Antonov An-124	CAT-A	H	D	J	330000	73,3	72,01646091	0,841753	16710479,6	16,71047957
3	A332	Airbus A-330-200	CAT-B	H	B	H	182000	60,3	69,44444444	0,840949	7796256,89	7,796256885
4	A333	Airbus A-330-300	CAT-B	H	B	H	187000	60,3	69,95884774	0,840719	8172231,12	8,172231116
5	A343	Airbus A-340-300	CAT-B	H	B	H	192000	60,3	69,95884774	0,840698	8615298,5	8,615298499
6	A345	Airbus A-340-500	CAT-B	H	B	H	246000	63,45	71,50205761	0,843913	12450188,4	12,45018836
7	A346	Airbus A-340-600	CAT-B	H	B	H	265000	63,45	74,07407407	0,843913	13946003,3	13,9460033
8	A359	Airbus A-350-900 XWB	CAT-B	H	B	H	207000	64,75	72,01646091	0,87448	8110822,4	8,110822401
9	B744	Boeing 747-400	CAT-B	H	B	H	285764	64,44	78,18930041	0,83775	15004716	15,00471603
10	B748	Boeing 747-8	CAT-B	H	B	H	312072	68,4	74,58847737	0,840181	16601157,9	16,60115791
11	B772	Boeing 777-200	CAT-B	H	B	H	201800	60,93	72,01646091	0,841267	9048982,2	9,048982205
12	B773	Boeing 777-300	CAT-B	H	B	H	237680	60,93	76,64609053	0,841267	11794633,6	11,79463363
13	B77L	Boeing 777-200LR	CAT-B	H	B	H	223168	64,8	72,01646091	0,843328	9760469,29	9,760469289
14	B77W	Boeing 777-300ER	CAT-B	H	B	H	251290	64,8	76,64609053	0,843328	11627839,7	11,62783971
15	B788	Boeing 787-8	CAT-B	H	B	H	172365	60,12	74,58847737	0,839557	6560297,64	6,560297642
16	B789	Boeing 787-9	CAT-B	H	B	H	192776	60,12	78,7037037	0,839557	7776924,4	7,7769244
17	IL96	Ilyushin Il-96-300	CAT-B	H	D	H	175000	55,57	77,16049383	0,835544	7688053,43	7,68805343
18	A306	Airbus A-300-600	CAT-C	H	C	H	140000	44,84	71,50205761	0,829161	8217745,45	8,217745446
19	A310	Airbus A-310	CAT-C	H	C	H	124000	43,9	71,50205761	0,826372	6748470,74	6,748470737
20	B703	Boeing 707-320B	CAT-C	H	D	H	97500	44,42	65,8436214	0,845458	4325452,99	4,325452987
21	B752	Boeing 757-200	CAT-C	M	E	UM	95250	38,05	70,47325103	0,842451	5275175,61	5,275175608
22	B753	Boeing 757-300	CAT-C	M	E	UM	101610	38,06	73,04526749	0,84246	5788676,61	5,788676606
23	B762	Boeing 767-200	CAT-C	H	C	H	123377	47,57	68,41563786	0,839657	5852346,27	5,852346273
24	B763	Boeing 767-300	CAT-C	H	C	H	136078	47,57	72,01646091	0,839657	6763337,25	6,763337245
25	B764	Boeing 767-400ER	CAT-C	H	C	H	158757	51,92	77,16049383	0,842741	7186092,66	7,18609266
26	C135	Boeing C-135	CAT-C	H	D	UM	106600	39,9	77,16049383	0,832549	5553275,82	5,553275819
27	DC10	McDonnell Douglas DC-10-30	CAT-C	H	C	H	186427	47,35	76,64609053	0,831873	12151116,5	12,15111646
28	DC85	Douglas DC-8-50	CAT-C	H	D	H	98431	43,4	70,47325103	0,847866	4302472,41	4,302472415
29	IL76	Ilyushin Il-76	CAT-C	H	D	H	152000	50,5	61,72839506	0,840387	8728216,76	8,728216756
30	MD11	McDonnell Douglas MD-11	CAT-C	H	C	H	195048	51,97	81,79012346	0,878331	9799495,1	9,799495099
31	A318	Airbus A-318	CAT-D	M	F	LM	57500	34,1	64,30041152	0,833181	2652522,2	2,652522197
32	A319	Airbus A-319	CAT-D	M	F	LM	62500	34,1	66,87242798	0,829596	3026375,88	3,026375884
33	A320	Airbus A-320	CAT-D	M	F	LM	66000	35,8	70,47325103	0,911656	2643943,1	2,643943103
34	A321	Airbus A-321	CAT-D	M	F	LM	77800	34,1	72,5308642	0,830165	4320646,52	4,32064652
35	AN12	Antonov An-12	CAT-D	M	/	LM	58000	38	62,75720165	0,770438	2408091,12	2,408091116
36	B736	Boeing 737-600	CAT-D	M	F	LM	55111	34,32	64,81481481	0,834203	2383534,05	2,383534053
37	B737	Boeing 737-700	CAT-D	M	F	LM	58604	34,32	67,90123457	0,834203	2572740,07	2,572740074
38	B738	Boeing 737-800	CAT-D	M	F	LM	66361	34,32	73,04526749	0,834203	3066569,57	3,066569574
39	B739	Boeing 737-900	CAT-D	M	F	LM	66814	34,32	72,5308642	0,834203	3130625,77	3,13062577
40	C130	Lockheed C-130J	CAT-D	M	F	LM	75000	40,41	66,87242798	0,834629	3084534,03	3,084534031
41	IL18	Ilyushin Il-18	CAT-D	M	/	LM	52600	37,4	66,87242798	0,843379	1752845,41	1,752845407
42	MD81	McDonnell Douglas MD-81	CAT-D	M	/	LM	58061	32,85	42,45923913	0,839681	4379225,12	4,379225121
43	MD82	McDonnell Douglas MD-82	CAT-D	M	F	LM	58567	32,85	69,95884774	0,839681	2704355,4	2,7043554
44	MD83	McDonnell Douglas MD-83	CAT-D	M	F	LM	63276	32,85	70,47325103	0,839681	3133676,67	3,133676666
45	MD87	McDonnell Douglas MD-87	CAT-D	M	F	LM	58060	32,85	72,01646091	0,839681	2581800,87	2,581800874
46	MD88	McDonnell Douglas MD-88	CAT-D	M	F	LM	58567	32,85	66,87242798	0,839681	2829171,8	2,829171803
47	MD90	McDonnell Douglas MD-90	CAT-D	M	F	LM	64410	32,87	70,98765432	0,839702	3219469,72	3,219469724
48	T204	Tupolev Tu-204	CAT-D	M	/	LM	89500	40,3	72,01646091	0,8968	3816754,3	3,816754297
49	AT43	ATR-42-300	CAT-E	M	G	L	16000	24,57	61,72839506	0,762121	450511,724	0,450511724
50	AT45	ATR-42-500	CAT-E	M	/	S	18300	24,57	56,58436214	0,762121	642919,906	0,642919906
51	AT72	ATR-72	CAT-E	M	G	S	22350	27,05	61,72839506	0,76669	720943,083	0,720943083
52	B712	Boeing 717-200	CAT-E	M	F	LM	46269	28,4	71,50205761	0,834372	2223570,21	2,223570209
53	B732	Boeing 737-200	CAT-E	M	F	LM	48534	28,35	66,87242798	0,826355	2650680,89	2,650680892
54	B733	Boeing 737-300	CAT-E	M	F	LM	52889	28,88	69,44444444	0,827962	2915236,11	2,915236108
55	B734	Boeing 737-400	CAT-E	M	F	LM	56245	28,88	71,50205761	0,827962	3202062,71	3,202062715
56	B735	Boeing 737-500	CAT-E	M	F	LM	49895	28,88	65,32921811	0,827962	2757954,68	2,757954675
57	CL60	Bombardier Challenger 650	CAT-E	M	G	S	17237	19,6	66,87242798	0,895555	645442,191	0,645442191
58	CRJ1	Canadair CRJ-100	CAT-E	M	G	S	20276	21,23	69,44444444	0,902878	727082,356	0,727082356
59	CRJ2	Canadair CRJ-200	CAT-E	M	G	S	21319	21,23	72,01646091	0,902878	775101,241	0,775101241
60	CRJ7	Canadair CRJ-700	CAT-E	M	G	S	30391	23,25	69,44444444	0,902315	1362805,45	1,362805454
61	CRJ9	Canadair CRJ-900	CAT-E	M	G	S	33340	23,24	69,44444444	0,902996	1640291,99	1,640291993
62	DH8D	De Havilland DHC-8 Q400	CAT-E	M	F	S	28123	28,4	62,24279835	0,768027	1025194,61	1,025194607
63	E135	Embraer ERJ-135	CAT-E	M	G	S	18500	20,04	66,87242798	0,837542	760466,133	0,760466133
64	E145	Embraer ERJ-145	CAT-E	M	G	S	18700	20,04	69,44444444	0,837773	748013,451	0,748013451
65	E170	Embraer ERJ-170	CAT-E	M	G	S	33300	26	66,87242798	0,926725	1322906,9	1,322906902
66	E175	Embraer ERJ-175	CAT-E	M	/	S	34000	26	66,87242798	0,926725	1379109,18	1,37910918
67	E190	Embraer ERJ-190	CAT-E	M	F	LM	44000	28,72	67,38683128	0,9234	1885197,02	1,885197024
68	E195	Embraer ERJ-195	CAT-E	M	/	LM	45800	28,72	69,44444444	0,923752	1981320,52	1,981320518
69	F70	Fokker 70	CAT-E	M	/	LM	34020	28,076	66,35802469	0,835732	1323192,95	1,323192952
70	F100	Fokker 100	CAT-E	M	/	LM	38780	28,076	66,35802469	0,835732	1719373,27	1,719373267
71	GLF4	Gulfstream 4	CAT-E	M	G	S	26535	23,7	72,01646091	0,934444	930983,479	0,930983479
72	RJ85	Avro RJ-85	CAT-E	M	/	LM	38555	26,21	64,30041152	0,815803	2061645,21	2,061645213
73	RJ1H	Avro RJ-100	CAT-E	M	/	LM	40143	26,21	64,30041152	0,815803	2234972,41	2,234972408
74	FA10	Dassault Falcon 10	CAT-F	M	/	L	8000	13,08	56,58436214	0,825275	400363,714	0,400363714
75	FA20	Dassault Falcon 20	CAT-F	M	/	L	12580	15,4	56,58436214	0,816236	722093,203	0,722093203
76	D328	Dornier 328	CAT-F	M	/	L	14390	20,98	56,58436214	0,751814	552699,622	0,552699622
77	E120	Embraer EMB-120	CAT-F	M	H	L	11700	19,78	64,81481481	0,762111	354007,13	0,35400713
78	BE40	Beechcraft Beechjet 400A	CAT-F	M	H	L	7120	13,3	61,72839506	0,816393	284222,227	0,284222227
79	H25B	Raytheon Hawker 800	CAT-F	M	H	L	10590	16,6	64,30041152	0,82941	381397,519	0,381397519
80	JS32	British Aerospace Jetstream 32	CAT-F	M	/	L	7080	15,85	59,1563786	0,759903	221836,786	0,221836786
81	JS41	British Aerospace Jetstream 41	CAT-F	M	/	L	10569	18,42	61,72839506	0,767484	347312,011	0,347312011
82	LJ35	Learjet 35	CAT-F	M	H	L	6940	12,04	64,30041152	0,809681	318950,926	0,318950926
83	LJ60	Learjet 60	CAT-F	M	H	L	8845	13,4	72,01646091	0,916056	330078,682	0,330078682
84	SF34	Saab 340	CAT-F	M	G	L	12930	21,44	59,1563786	0,768456	399863,773	0,399863773
85	P180	Piaggio P-180 Avanti	CAT-F	L	I	L	4965	14,03	61,72839506	0,811408	124963,786	0,124963786
86	C650	Cessna 650	CAT-F	M	/	L	8618	16,31	66,87242798	0,827866	252048,071	0,252048071
87	C525	Cessna 525	CAT-F	L	I	L	4445	14,3	56,58436214	0,829715	102856,48	0,10285648
88	C180	Cessna 180	CAT-F	L	/	L	1275	11	33,43621399	0,771108	26042,826	0,026042826
89	C152	Cessna 152	CAT-F	L	/	L	760	10,2	28,29218107	0,767968	12770,343	0,012770343

Appendix B – Calculation of the Oswald Factor without Input of C_{D0}

Index	Model	wing span [m]	fuselage diameter [m]	winglet height [m]	taper ratio [-]	sweep angle [deg]	aspect ratio [-]	k_e_F [-]	k_e_WL [-]	e_theo [-]	Oswald Factor [-]
1	Airbus A-380-800	79,75	7,14	0	0,225240521	30	7,79	0,983969	1	0,983773	0,845065387
2	Antonov An-124	73,3	6,4	0	0,286	27	8,79	0,984753	1	0,979136	0,841752911
3	Airbus A-330-200	60,3	5,64	0	0,232954545	29,7	9,26	0,982503	1	0,980441	0,840949446
4	Airbus A-330-300	60,3	5,64	0	0,237689394	29,7	9,26	0,982503	1	0,980172	0,840718659
5	Airbus A-340-300	60,3	5,64	0	0,238095238	29,7	9,26	0,982503	1	0,980149	0,84069844
6	Airbus A-340-500	63,45	5,64	0	0,219211823	31,1	8,56	0,984198	1	0,982203	0,843913405
7	Airbus A-340-600	63,45	5,64	0	0,219211823	31,1	8,56	0,984198	1	0,982203	0,843913405
8	Airbus A-350-900 XWB	64,75	5,96	2,88	0,384558278	31,9	11,84339689	0,983055	1,0638556	0,957801	0,874479965
9	Boeing 747-400	64,44	6,5	0	0,275	38	7,39	0,979651	1	0,979555	0,837749634
10	Boeing 747-8	68,4	6,5	0	0,221088435	38	8,644789357	0,981939	1	0,980108	0,840180637
11	Boeing 777-200	60,93	6,2	0	0,149	31,6	8,67	0,979291	1	0,984028	0,841266981
12	Boeing 777-300	60,93	6,2	0	0,149	31,6	8,67	0,979291	1	0,984028	0,841266981
13	Boeing 777-200LR	64,8	6,2	0	0,149	31,6	8,67	0,981691	1	0,984028	0,843328431
14	Boeing 777-300ER	64,8	6,2	0	0,149	31,6	8,67	0,981691	1	0,984028	0,843328431
15	Boeing 787-8	60,12	5,77	0	0,18	32,2	10,58	0,981578	1	0,979741	0,839557264
16	Boeing 787-9	60,12	5,77	0	0,18	32,2	10,58	0,981578	1	0,979741	0,839557264
17	Ilyushin Il-96-300	55,57	6,08	0	0,279	30	7,89	0,976058	1	0,980572	0,835543948
18	Airbus A-300-600	44,84	5,64	0	0,292553191	28	7,73	0,968359	1	0,980818	0,829161302
19	Airbus A-310	43,9	5,64	0	0,283	28	8,8	0,966989	1	0,978904	0,826372405
20	Boeing 707-320B	44,42	3,76	0	0,259	35	6,96	0,98567	1	0,982531	0,845458322
21	Boeing 757-200	38,05	3,76	0	0,243	25	7,82	0,98047	1	0,984229	0,842451298
22	Boeing 757-300	38,06	3,76	0	0,243	25	7,82	0,980481	1	0,984229	0,842460115
23	Boeing 767-200	47,57	5,03	0	0,207	31,5	7,99	0,977639	1	0,983806	0,83965736
24	Boeing 767-300	47,57	5,03	0	0,207	31,5	7,99	0,977639	1	0,983806	0,83965736
25	Boeing 767-400ER	51,92	5,03	0	0,207	31,5	7,99	0,981229	1	0,983806	0,84274071
26	Boeing C-135	39,9	4,2	0	0,35483871	36	7,044292035	0,977839	1	0,975277	0,832548918
27	McDonnell Douglas DC-10-30	47,35	6,02	0	0,22	35	6,91	0,967672	1	0,984724	0,831872657
28	Douglas DC-8-50	43,4	3,73	0	0,181	30	7,52	0,985227	1	0,985773	0,847866195
29	Ilyushin Il-76	50,5	4,8	0	0,290322581	25	8,5	0,981931	1	0,980356	0,840386944
30	McDonnell Douglas MD-11	51,97	6	1,93	0,239	35	7,91	0,973342	1,053179	0,981469	0,878331364
31	Airbus A-318	34,1	3,95	0	0,247116969	25	9,500081699	0,973164	1	0,980707	0,833181345
32	Airbus A-319	34,1	3,95	0	0,247116969	25	11,6281	0,973164	1	0,976487	0,829596102
33	Airbus A-320	35,8	3,95	2,43	0,24	25	12,8164	0,975652	1,0982404	0,974595	0,911655574
34	Airbus A-321	34,1	3,95	0	0,247116969	25	11,28941748	0,973164	1	0,977156	0,830164642
35	Antonov An-12	38	3,9	0	0,391304348	8,5	10,6	0,978934	1	0,978878	0,770437997
36	Boeing 737-600	34,32	3,76	0	0,278	25	9,44	0,975994	1	0,979062	0,834203033
37	Boeing 737-700	34,32	3,76	0	0,278	25	9,44	0,975994	1	0,979062	0,834203033
38	Boeing 737-800	34,32	3,76	0	0,278	25	9,44	0,975994	1	0,979062	0,834203033
39	Boeing 737-900	34,32	3,76	0	0,278	25	9,44	0,975994	1	0,979062	0,834203033
40	Lockheed C-130J	40,41	4,34	0	0,512820513	1,5	10,07383159	0,976931	1	0,978623	0,834629159
41	Ilyushin Il-18	37,4	3,23	0	0,363636364	2,5	10	0,985083	1	0,9807	0,843379349
42	McDonnell Douglas MD-81	32,85	3,35	0	0,195	24,5	9,62	0,979201	1	0,982264	0,839680721
43	McDonnell Douglas MD-82	32,85	3,35	0	0,195	24,5	9,62	0,979201	1	0,982264	0,839680721
44	McDonnell Douglas MD-83	32,85	3,35	0	0,195	24,5	9,62	0,979201	1	0,982264	0,839680721
45	McDonnell Douglas MD-87	32,85	3,35	0	0,195	24,5	9,62	0,979201	1	0,982264	0,839680721
46	McDonnell Douglas MD-88	32,85	3,35	0	0,195	24,5	9,62	0,979201	1	0,982264	0,839680721
47	McDonnell Douglas MD-90	32,87	3,35	0	0,195	24,5	9,62	0,979226	1	0,982264	0,839702419
48	Tupolev Tu-204	40,3	4,1	1,91	0,228	28	8,8169924	0,979299	1,0681106	0,982086	0,896799558
49	ATR-42-300	24,57	2,865	0	0,533333333	2	11,07678716	0,972806	1	0,97441	0,762121046
50	ATR-42-500	24,57	2,865	0	0,533333333	2	11,07678716	0,972806	1	0,97441	0,762121046
51	ATR-72	27,05	2,865	0	0,47	3,5	11,99512295	0,977564	1	0,975481	0,766690243
52	Boeing 717-200	28,4	3,4	0	0,196	24,5	8,68	0,971335	1	0,983957	0,834371662
53	Boeing 737-200	28,35	3,76	0	0,266	25	8,83	0,96482	1	0,981085	0,826355442
54	Boeing 737-300	28,88	3,76	0	0,24	25	9,17	0,966099	1	0,98169	0,827962137
55	Boeing 737-400	28,88	3,76	0	0,24	25	9,17	0,966099	1	0,98169	0,827962137
56	Boeing 737-500	28,88	3,76	0	0,24	25	9,17	0,966099	1	0,98169	0,827962137
57	Bombardier Challenger 650	19,6	2,41	1,29	0,333333333	28	8,456086287	0,969762	1,0951901	0,975941	0,895554795
58	Canadair CRJ-100	21,23	2,69	1,29	0,288	24,75	7,72	0,96789	1,0877282	0,982354	0,902877538
59	Canadair CRJ-200	21,23	2,69	1,29	0,288	24,75	7,72	0,96789	1,0877282	0,982354	0,902877538
60	Canadair CRJ-700	23,25	2,69	1,29	0,26	26,5	7,655608271	0,973228	1,07996	0,983381	0,902314801
61	Canadair CRJ-900	23,24	2,69	1,29	0,25	26	7,59951597	0,973204	1,079995	0,984114	0,902995646
62	De Havilland DHC-8	28,4	2,96	0	0,38	3,1	12,7822504	0,978274	1	0,976472	0,768027156
63	Embraer ERJ-135	20,04	2,28	0	0,25	21,5	7,8	0,974112	1	0,98488	0,837541698
64	Embraer ERJ-145	20,04	2,28	0	0,231	22,73	7,8	0,974112	1	0,985152	0,837772786
65	Embraer ERJ-170	26	3,01	2	0,29	22,5	8,6	0,973195	1,1116805	0,981198	0,926724794
66	Embraer ERJ-175	26	3,01	2	0,29	22,5	8,6	0,973195	1,1116805	0,981198	0,926724794
67	Embraer ERJ-190	28,72	3,01	2	0,27	25	8,1	0,978032	1,1008501	0,982414	0,92340046
68	Embraer ERJ-195	28,72	3,01	2	0,28	22,5	8,1	0,978032	1,1008501	0,982788	0,923751646
69	Fokker 70	28,076	3,3	0	0,235	17,45	8,43060723	0,97237	1	0,984513	0,835731762
70	Fokker 100	28,076	3,3	0	0,235	17,45	8,43060723	0,97237	1	0,984513	0,835731762
71	Gulfstream 4	23,7	2,21	2	0,357142857	28	6,361155153	0,982609	1,1228333	0,980264	0,934443673
72	Avro RJ-85	26,21	3,56	0	0,356	15	8,89	0,963103	1	0,98039	0,815802583
73	Avro RJ-100	26,21	3,56	0	0,356	15	8,89	0,963103	1	0,98039	0,815802583
74	Dassault Falcon 10	13,08	1,42	0	0,342857143	30	7,099020747	0,976428	1	0,978238	0,825275092
75	Dassault Falcon 20	15,4	1,98	0	0,386	30	6,5	0,966939	1	0,977019	0,816235622
76	Dornier 328	20,98	2,17	0	0,7	2,5	11,00401	0,978604	1	0,955537	0,751814008
77	Embraer EMB-120	19,78	2,28	0	0,55	3,5	9,922607152	0,973427	1	0,973776	0,762111018
78	Beechcraft Beechjet 400A	13,3	1,76	0	0,368	20	7,827	0,964977	1	0,979193	0,816392616
79	Raytheon Hawker 800	16,6	1,83	0	0,322	20	7,057	0,975694	1	0,98388	0,829410471
80	British Aerospace Jetstream 32	15,85	1,98	0	0,33	0,7	10,01684609	0,968789	1	0,975602	0,759903114
81	British Aerospace Jetstream 41	18,42	1,98	0	0,347826087	1	10,41105861	0,976891	1	0,977163	0,767483666
82	Learjet 35	12,04	1,5	0	0,655172414	14	6,160713982	0,968957	1	0,967153	0,809680598
83	Learjet 60	13,4	1,81	1,15	0,419354839	16,5	7,631109222	0,96351	1,1249801	0,978155	0,916056397
84	Saab 340	21,44	2,31	0	0,4	4,5	11,65796602	0,976783	1	0,97851	0,768456404
85	Piaggio P-180 Avanti	14,03	1,85	0	0,34	1	11,96	0,965226	1	0,972964	0,811408196
86	Cessna 650	16,31	1,5	0	0,344827586	26	8,94	0,983084	1	0,974666	0,82786586
87	Cessna 525	14,3	1,47	0	0,346153846	2	9,1	0,978865	1	0,981052	0,829714651
88	Cessna 180	11	1,07	0	0,64	0	7,487623762	0,981076	1	0,977589	0,771107946
89	Cessna 152	10,2	1,02	0	0,692307692	0,5	6,936	0,98	1	0,974678	0,767968195

Appendix C – Calculation of the Oswald Factor with Input of C_{D0}

Index	Model	e_theo [-]	k_e_F	Aspect ratio [-]	S_wet [m^2]	S_ref [m^2]	C_D_0 [-]	Q	Oswald Factor M2 [-]
1	Airbus A-300-600	0,980818	0,9794	7,73	1569,11	260	0,018105	1,041	0,827760132
2	Airbus A-310	0,978904	0,9824	8,8	1342,81	219	0,018395	1,03985	0,810965162
3	Airbus A-320	0,967854	0,9809	16,329681	791,13	122,4	0,01939	1,05334	0,698642049
4	Airbus A-321	0,976867	0,9735	11,43555728	874,15	122,4	0,021425	1,05154	0,744029465
5	Airbus A-340-300	0,980149	0,9842	9,26	2033,09	363,1	0,016798	1,03663	0,818110979
6	Boeing 737-300	0,98169	0,9657	9,17	645,85	105,4	0,018383	1,05481	0,796146667
7	Boeing 757-200	0,984229	0,9889	7,82	1113,79	185,25	0,018037	1,02741	0,836259419
8	Boeing 767-300	0,983806	0,9737	7,99	1580,69	283,3	0,016739	1,04387	0,830888593
9	Fokker 100	0,992049	0,9458	4,295204278	581,47	93,5	0,018657	1,06582	0,860968907
10	McDonnell Douglas MD-11	0,981469	0,9503	7,91	2051,8	338,9	0,018163	1,0722	0,80404312
11	McDonnell Douglas MD-87	0,982264	0,9845	9,62	742,27	112,3	0,019829	1,03413	0,79248343
12	McDonnell Douglas MD-90	0,982264	0,9731	9,62	818,79	112,3	0,021873	1,04621	0,770765055